
Simulated Tornado Wind Fields and Damage Patterns

Prepared by D. R. Metcalf, R. E. Peterson

Atmospheric Science Group
Texas Tech University

Prepared for
U.S. Nuclear Regulatory
Commission

NOTICE

This report was prepared as an account of work sponsored by an agency of the United States Government. Neither the United States Government nor any agency thereof, or any of their employees, makes any warranty, expressed or implied, or assumes any legal liability or responsibility for any third party's use, or the results of such use, of any information, apparatus product or process disclosed in this report, or represents that its use by such third party would not infringe privately owned rights.

Available from

GPO Sales Program
Division of Technical Information and Document Control
U. S. Nuclear Regulatory Commission
Washington, D. C. 20555

Printed copy price: \$4.75

and

National Technical Information Service
Springfield, Virginia 22161

Simulated Tornado Wind Fields and Damage Patterns

Manuscript Completed: August 1978
Date Published: February 1982

Prepared by
D. R. Metcalf, R. E. Peterson

Atmospheric Science Group
Texas Tech University
P.O. Box 4320
Lubbock, TX 79409

Prepared for
Division of Health, Siting and Waste Management
Office of Nuclear Regulatory Research
U.S. Nuclear Regulatory Commission
Washington, D.C. 20555
NRC FIN B6177
Under Contract No. NRC-04-77-106

Availability of Reference Materials Cited in NRC Publications

Most documents cited in NRC publications will be available from one of the following sources:

1. The NRC Public Document Room, 1717 H Street, N.W.
Washington, DC 20555
2. The NRC/GPO Sales Program, U.S. Nuclear Regulatory Commission,
Washington, DC 20555
3. The National Technical Information Service, Springfield, VA 22161

Although the listing that follows represents the majority of documents cited in NRC publications, it is not intended to be exhaustive.

Referenced documents available for inspection and copying for a fee from the NRC Public Document Room include NRC correspondence and internal NRC memoranda; NRC Office of Inspection and Enforcement bulletins, circulars, information notices, inspection and investigation notices; Licensee Event Reports; vendor reports and correspondence; Commission papers; and applicant and licensee documents and correspondence.

The following documents in the NUREG series are available for purchase from the NRC/GPO Sales Program: formal NRC staff and contractor reports, NRC-sponsored conference proceedings, and NRC booklets and brochures. Also available are Regulatory Guides, NRC regulations in the *Code of Federal Regulations*, and *Nuclear Regulatory Commission Issuances*.

Documents available from the National Technical Information Service include NUREG series reports and technical reports prepared by other federal agencies and reports prepared by the Atomic Energy Commission, forerunner agency to the Nuclear Regulatory Commission.

Documents available from public and special technical libraries include all open literature items, such as books, journal and periodical articles, and transactions. *Federal Register* notices, federal and state legislation, and congressional reports can usually be obtained from these libraries.

Documents such as theses, dissertations, foreign reports and translations, and non-NRC conference proceedings are available for purchase from the organization sponsoring the publication cited.

Single copies of NRC draft reports are available free upon written request to the Division of Technical Information and Document Control, U.S. Nuclear Regulatory Commission, Washington, DC 20555.

Copies of industry codes and standards used in a substantive manner in the NRC regulatory process are maintained at the NRC Library, 7920 Norfolk Avenue, Bethesda, Maryland, and are available there for reference use by the public. Codes and standards are usually copyrighted and may be purchased from the originating organization or, if they are American National Standards, from the American National Standards Institute, 1430 Broadway, New York, NY 10018.

ABSTRACT

The translational motion as well as the internal motions of the tornado combine to produce the forces experienced by a structure. The combined wind flow and damage patterns are investigated in a series of numerical simulations. The results have been studied and organized on the basis of characteristic properties. Analysis of the damage patterns generated by the simulated tornado wind fields are performed and compared with actual, observed tornado damage patterns. An attempt has been made to categorize tornado damage patterns so that they might be used in field investigations of tornado damage. Various hypothetical sequences of tornado development and behavior are proposed to simulate the resulting tornado damage patterns.

TABLE OF CONTENTS

ABSTRACT	iii
LIST OF FIGURES	vii
I. INTRODUCTION	1
II. SURVEY OF LITERATURE	3
III. FORMULATION	7
IV. METHOD OF SOLUTION	13
V. RESULTS AND DISCUSSION	16
VI. CONCLUSION	63
LIST OF REFERENCES	66

LIST OF FIGURES

Figure

1. Geometry for a translating vortex, illustrating wind components and angles in the computation of the total flow field.	8
2. Isotachs and streamlines for $G_{MAX} = 1$ and $\beta = 30^\circ$ for a Rankine vortex	18
3. Isotachs and streamlines for $G_{MAX} = 4$ and $\beta = 30^\circ$ for a Rankine vortex	19
4. Isotachs and streamlines for $G_{MAX} = 6$ and $\beta = 30^\circ$ for a Rankine vortex	20
5. Isotachs and streamlines for $G_{MAX} = 4$ and $\beta = 0^\circ$ for a Rankine vortex	21
6. Isotachs and streamlines for $G_{MAX} = 4$ and $\beta = -30^\circ$ for a Rankine vortex	23
7. Isotachs and streamlines for $G_{MAX} = 4$ and $\beta = 60^\circ$ for a Rankine vortex	24
8. Isotachs and streamlines for $G_{MAX} = 4$ and $\beta = 90^\circ$ for a Rankine vortex	25
9. Percentage of the vortex field experiencing relative calm, $ V_{TOT} < V_{TRAN} $ (after Letzmann, 1924).	26
10. Isotachs and streamlines for $G_{MAX} = 4$ and $\beta = 30^\circ$ for a potential vortex	27
11. Isotachs and streamlines for $G_{MAX} = 0.5$ and $\beta = 60^\circ$ for a solid rotation core.	29
12. Streamlines for a Rankine-like, two-cell vortex in translation	30
13. Isotachs and streamlines for $G_{MAX} = 4$, $\beta = 30^\circ$, and a shear of 45°	31
14. Isotachs and streamlines for $G_{MAX} = 4$, $\beta = 30^\circ$, and a shear of 14°	33
15. Isotachs and streamlines for $G_{MAX} = 4$, $\beta = 30^\circ$, and curvature (Q) = 1.	34
16. Isotachs and streamlines for $G_{MAX} = 4$, $\beta = 30^\circ$, and curvature (Q) = 4.	35
17. Isotachs and streamlines for $G_{MAX} = 4$, $\beta = 30^\circ$, shear of 7° , and curvature (Q) = 8.25	37
18. Isotachs and streamlines for $G_{MAX} = 4$, $\beta = 30^\circ$, shear of 45° , and curvature (Q) = 1	38

Figure

19.	Swath diagrams for a range of G_{CRIT} and β for $G_{MAX} = 4$. . .	39
20.	Examples of early damage swaths by ground survey.	42
21.	Damage swath for $G_{MAX} = 4$, $\beta = 30^\circ$, and $G_{CRIT} = 0.8$	43
22.	Damage swath for $G_{MAX} = 4$, $\beta = 30^\circ$, and $G_{CRIT} = 1.6$	44
23.	Damage swath for $G_{MAX} = 4$, $\beta = 30^\circ$, and $G_{CRIT} = 2.4$	45
24.	Damage swath for $G_{MAX} = 4$, $\beta = 30^\circ$, and $G_{CRIT} = 3.2$	46
25.	Damage swath for $G_{MAX} = 4$, $\beta = 30^\circ$, and $G_{CRIT} = 4.0$	47
26.	Damage swath for $G_{MAX} = 4$ and $\beta = 30^\circ$ for a sequence of different G_{CRIT}	48
27.	Damage swaths for $G_{MAX} = 4$, β increasing from 0° to 90° and for $G_{CRIT} = 0.8, 1.6, \text{ and } 2.4$	49
28.	Damage swath with G_{MAX} increasing from 1.0 to 10.0, $\beta =$ 30° , and $G_{CRIT} = 1.6$	50
29.	Damage swath for an evolving vortex for $G_{CRIT} = 1.8$ with varying G_{MAX} and β	52
30.	Damage swath for $G_{MAX} = 4$, $\beta = 30^\circ$, and G_{CRIT} increasing left to right from 0.5 to 4.0	53
31.	Damage swath for $G_{MAX} = 4$, $\beta = 30^\circ$, and G_{CRIT} decreasing left to right from 4.0 to 0.5	54
32.	Damage swath for $G_{MAX} = 4$, $\beta = 30^\circ$, and G_{CRIT} increasing from 0.5 on the sides to 4.0 along the centerline	56
33.	Characteristic swath types (after Letzmann, 1924)	57
34.	Isotachs, streamlines, and damage swaths for the NRC vortex	59
35.	Isotachs, streamlines, and damage swaths for Fujita's DBT-77.	60
36.	Isotachs and streamlines for the subvortices model.	61

Acknowledgments

The advice, guidance, and suggestions of our colleagues at Texas Tech University, Atmospheric Science Group, Drs. Gerald Jurica and Donald Haragan, are gratefully acknowledged. We would also like to express our appreciation to Robert F. Abbey, Jr., Office of Nuclear Regulatory Research, USNRC for his monitoring of our contract, NRC-04-77-106. Charmayne Klett contributed many hours of her time typing this manuscript; her effort increased the quality of the product.

CHAPTER I

INTRODUCTION

Tornadoes are the most locally destructive storms in nature. Protection from their devastating effect requires safeguards to save lives and minimize property damage. Substantially less property damage and virtually no loss of life would occur if structures were made of steel-reinforced concrete one meter thick; however, the cost would be prohibitive, even without regard to the appearance of the structure. Attempts must be made to understand the tornado so that structures with adequate strength to withstand the effects of the storm can be designed at an affordable cost. Increased understanding of the near-ground tornado winds will aid engineers in designing structures that may only need to survive the "average" tornado instead of always having to design for the "Maximum" tornado. Engineers will benefit from this study by recognizing the kinds of wind field patterns that can occur in tornadoes. Scientists may be able to interpret internal tornado configuration from the different damage patterns recorded. The principle objective of this study is to better understand these near-ground tornado wind fields and the damage patterns associated with them.

The translational motion as well as the internal motions of the tornado combine to produce the forces experienced by a structure. The combined wind flow and damage patterns are investigated in a series of numerical simulations. The results have been studied and organized on the basis of characteristic properties.

The basic tornado model used is the combined-Rankine vortex or Rankine vortex. This model implies solid rotation in the core (where velocity is proportional to the distance from the vortex center). This induces a potential flow outside the tornado core which is characterized by a velocity decreasing with increasing distance from the vortex center. A computer model based on this formulation is used to generate the combined horizontal wind fields. Since there are

virtually no stationary tornadoes, translational motion is then added vectorially to the rotational wind field produced by the vortex. Several cases were investigated. The simplest case is the uniform rectilinear translation; more complicated cases with curvature and/or shear are incorporated in the translational motion. An idealized case of a tornado cyclone with sub-vortices is also presented.

The second portion of the thesis deals with damage patterns generated by the tornado wind field. Damage patterns or swaths are simulated using a failure criterion in which regular objects, such as trees, utility poles, etc., would fall if a specified wind speed existed. An attempt has been made to categorize tornado damage patterns so that they might be used in field investigations of tornado damage.

The final portion of the thesis deals with questions often arising regarding the swath pattern as a tornado passes over irregular objects or irregular terrain. What is the appearance of the swath if objects are of differing resistance? What is the appearance if the tornado is changing in strength? Various hypothetical sequences of tornado development are proposed to simulate the resulting tornado damage patterns.

CHAPTER II

SURVEY OF LITERATURE

Tornadoes have been mentioned in the great religious books and discussed by natural philosophers, such as Pliny the Elder, Seneca, and Lucretious (Brooks, 1951) since early times. However, it was not until the Seventeenth Century that the first scientific study appeared, (Peterson, 1977). In 1689, Fr. F. Lamy wrote a 169 page monograph that included investigations of damage along with interviews of eyewitnesses of damaging storms in France. Although tornado path maps probably existed earlier, the first map to appear in print was published in 1730 in a twenty-eight page report by R. Budget (Peterson, 1977).

According to a paper in The Monthly Review (Anon., 1750), Father Boscovich published a book that was a study of the tornado that struck Rome 11 June 1749. The book included sections on tornado theories and the account of the tornado that hit Rome along with accounts of a few other tornadoes. The contents of this book were widely recognized even in America. According to Ludlam (1970), Benjamin Franklin used the book as a basis for his waterspout model. In another significant aspect, the analysis by Boscovich enforced the concept that a tornado is a vortex with rotary winds. This concept, however, was not shared by all investigators. The historical collection of Ludlam reveals the controversy in America between William C. Redfield and James P. Espy regarding the role of rotation in tornadoes. Redfield felt that rotary motion was in existence in a tornado while Espy believed that a tornado was composed of only radial winds directed inward. Even after surveying the same tornado damage, each would draw evidence supporting his own theory.

It was not until the late Nineteenth and early Twentieth Centuries that researchers began to study translating vortices. It has been assumed earlier that stationary vortex models could be used in understanding translating ones. The Twentieth Century began with Wegener's (1917)

Wind-und Wasserhosen in Europa (Tornadoes and Waterspouts in Europe). In his book, hundreds of tornado reports were examined. Letzmann (1924; 1928; 1937) followed Wegener's work with more tornado track studies. Wegener believed that in order to explain the observed characteristics it was important to have the translational motion in addition to the vortex motion. He considered tornadoes to be one- or two-cell structures. A one-cell vortex has only convergent flow, while a two-cell vortex has a divergent core and a convergent outer region (Letzmann, 1924). Wegener used a graphical solution for a one-cell vortex in translation to obtain the general properties of the observed damage swath. Letzmann (1918; 1924) adopted some of Wegener's ideas and extended the research with other vortex wind distributions.

Most early tornado studies were recorded observations rather than actual measurements of tornado damage patterns. After Bosovich, Martins (1850) was one of the next to record the orientation of the damage. Wegener (1917) encouraged researchers to make detailed measurements at many locations across the damage swath, with special care in recording the direction of tree fall using a compass and grid paper. Letzmann (1928 and 1937) suggested additional guidelines for investigating tornado damage. These were rejected by the United States Weather Bureau (Kincer, 1937) as being too ambitious; however, similar techniques are used today in tornado investigations throughout the world. Several of the more significant guidelines are mentioned below:

1. Aerial photography should precede a general, organized ground investigation.
2. Observations by chance eyewitnesses should be recorded as accurately as possible, including all details of the clouds, the weather elements, the funnel and the tornado itself.
3. Daily newspapers should be collected concerning the tornado.
4. Suitable tools such as a drawing pad, compass, dividers, pencils, scaled paper, and tape measure should be used during the field investigation.

Many more guidelines exist that can contribute to a successful survey of tornado damage.

Knowing the tornado structures that might exist plays an important role in the interpretation of tornado damage swaths. Significant aspects of the vortex structure include low level inflow, rotational motion, pressure gradient forces, centrifugal forces, and the winds associated with the vortex. These factors all play a role in vortex evolution. It is also important to distinguish between a one-cell vortex and a multi-cell vortex. Numerous articles were reviewed in order to provide some insight with regard to the relationships among the vortex structure, life cycle, and damage patterns. Several of these models were tested against the tornado wind fields obtained here. One article, in particular, was used as a basis for testing the possible stages in the life cycle of a tornado.

V. M. Mal'bakhov (1972) described the life cycle of a vortex based on a numerical integration of the time dependent thermo-hydrodynamic equations. Five possible stages of the life cycle are discussed. The first stage consists of the development of a buoyant thermal updraft, characterized by strong ascending velocities near the axis of symmetry of the thermal and weak descending velocities outside the vortex proper. In this initial stage no rotational velocity nor pressure disturbances exist. The vortex is initiated by a thermal pulse only. The first stage is also regarded as "unicellular" or "single-cell" or "one-cell" meaning only upward components of velocity exist in the vortex. During the second stage of a vortex development rotational motion is initiated. A region with maximum rotational velocity forms in the middle and lower parts of the vortex near the axis of symmetry. The pressure near the vortex axis, particularly in the lower reaches, begins to decrease appreciably. The third stage may be termed the mature vortex, during which a transformation begins. A relatively narrow descending stream forms at the upper part of the vortex axis. Air particles at the lower end move away from the vortex axis and then join the ascending motion. The descending stream gradually increases in strength and propagates downward. This constitutes a "two-cell" vortex. The fourth stage of the vortex model is characterized by vortex attenuation. During this stage the maximum rotational

velocity decreases, the pressure field weakens and the descending flow weakens and may disappear entirely. At the end of this fourth stage, the vortex becomes "one-cell" again. In the fifth stage, the aging stage, all processes continue to attenuate resulting in destruction of the vortex.

Review of the literature reveals that one-cell and two-cell vortex structures are the most numerous. In addition, the Rankine vortex seems to have one of the most realistic horizontal wind field distributions used in the literature. Other wind field distributions appear to closely resemble this one.

CHAPTER III

FORMULATION

The formulation for the determination of translating tornado wind fields entails a unique system of parameters and variables. Before investigating the entire vortex, the stationary vortex components should be established. In the vortices studied here, the change in velocity as a function of radius is specified, including the inflow (or outflow) angle. With the addition of the translational velocity to the basic vortex, flow patterns are depicted from computations of total vector wind (speed and orientation). The geometry of the problem can be portrayed in several forms. The one chosen here, shown in Fig. 1, reveals the basic form of the system, which is a slight modification of the orientation used by Letzmann. The definitions of the variables in Fig. 1 are listed below along with other variables that are defined later.

V_{TRAN} \equiv translational velocity - reference for most other velocities and angles

$V(r)$ or V \equiv rotational velocity - velocity within a tornado and is the resultant of the tangential and radial components of the rotation

V_{MAX} \equiv maximum velocity - velocity reached in a non-translating rotational vortex

V_{TOT} \equiv total velocity - resultant of V_{TRAN} and $V(r)$ at a particular point

V_{CRIT} \equiv critical velocity - velocity at which an object will fail

V_{TANG} \equiv tangential velocity of stationary vortex

G $\equiv V(r)/V_{\text{TRAN}}$

G_{MAX} $\equiv V_{\text{MAX}}/V_{\text{TRAN}}$

G_{TOT} $\equiv V_{\text{TOT}}/V_{\text{TRAN}}$

G_{CRIT} $\equiv V_{\text{CRIT}}/V_{\text{TRAN}}$

P \equiv angle of the radius vector measured counterclockwise from V_{TRAN}

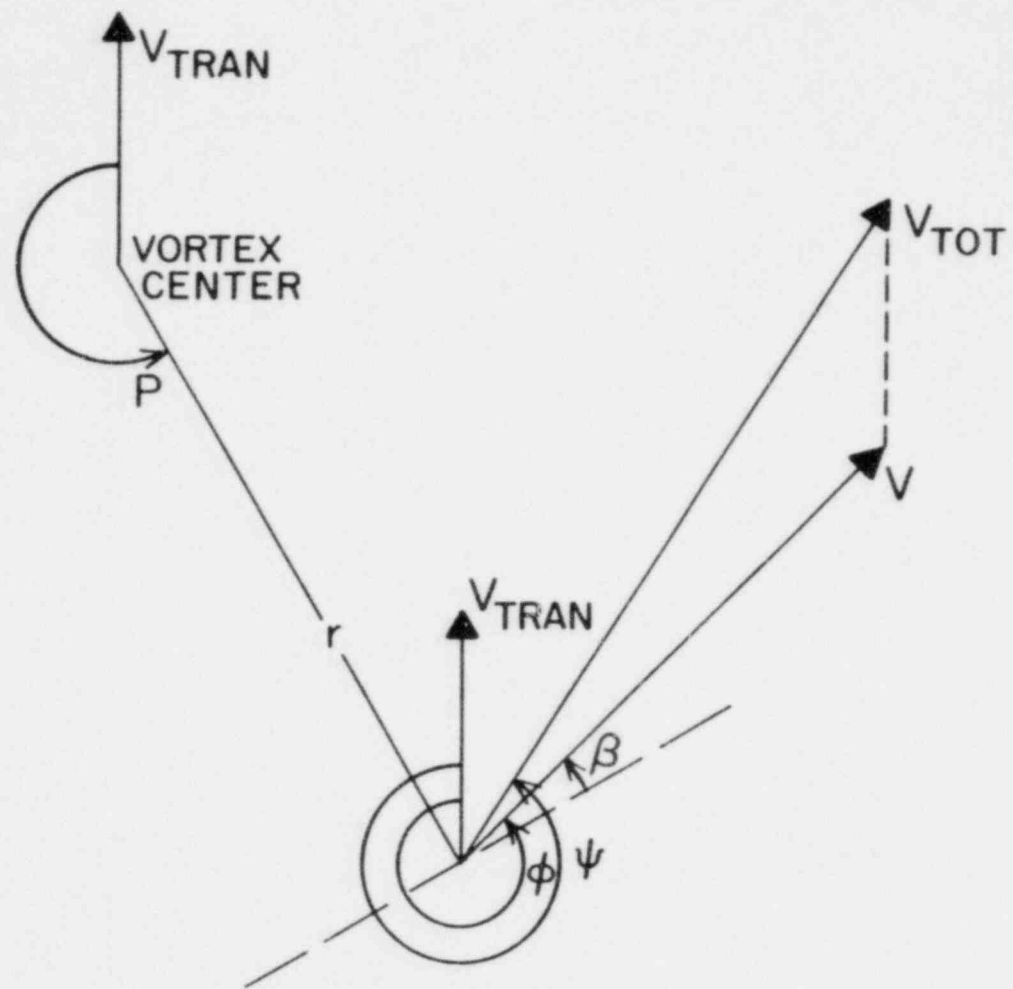


Fig. 1. Geometry for a translating vortex, illustrating wind components and angles in the computation of the total flow field.

$\beta \equiv$ angle of inflow for V ; measured counterclockwise from V_{TANG} to V

$\phi \equiv$ angle measured counterclockwise between V_{TRAN} and V

$\psi \equiv$ angle measured counterclockwise between V_{TRAN} and V_{TOT}

From the law of cosines,

$$V^2 = V_{TOT}^2 + V_{TRAN}^2 - 2 V_{TOT} V_{TRAN} \cos \psi$$

From the definition of V_{TOT}

$$V_{TOT}^2 = V_{TRAN}^2 + V^2 + 2 V_{TRAN} V \cos \phi$$

Specified parameters in these two equations include V , V_{TRAN} and ϕ ; unknown variables are V_{TOT} and ψ . The two unknown quantities are the most important if velocity fields and swath characteristics are to be established. Solving for V_{TOT} and ψ may be performed algebraically.

The steps are shown below. Rearranging the law of cosines yields

$$\cos \psi = \frac{V_{TRAN}^2 + V_{TOT}^2 - V^2}{2 V_{TOT} V_{TRAN}}$$

Substituting for V_{TOT}^2 gives

$$\begin{aligned} \cos \psi &= \frac{V_{TRAN}^2 - V^2 + V_{TRAN}^2 - V^2 + 2 V_{TRAN} V \cos \phi}{2 V_{TRAN} (V_{TRAN}^2 + V^2 - 2 V_{TRAN} V \cos \phi)^{\frac{1}{2}}}, \\ &= \frac{2 V_{TRAN}^2 + 2 V_{TRAN} V \cos \phi}{2 V_{TRAN} (V_{TRAN}^2 + V^2 + 2 V_{TRAN} V \cos \phi)^{\frac{1}{2}}}, \\ &= \frac{V_{TRAN} + V \cos \phi}{(V_{TRAN}^2 + V^2 + 2 V_{TRAN} V \cos \phi)^{\frac{1}{2}}} = \frac{V_{TRAN} + V \cos \phi}{V_{TOT}}. \end{aligned}$$

Now, normalization of the two principle equations in terms of V_{TRAN} yields

$$\frac{V_{TOT}^2}{V_{TRAN}^2} = \frac{V_{TRAN}^2}{V_{TRAN}^2} + \frac{V^2}{V_{TRAN}^2} + \frac{2 V_{TRAN} V \cos \phi}{V_{TRAN}^2}.$$

which in turn yields

$$G_{TOT}^2 = 1 + G^2 + 2 G \cos \phi.$$

and

$$\cos \psi = \frac{\frac{V_{TRAN}}{V_{TRAN}} + \frac{V \cos \phi}{V_{TRAN}}}{\frac{V_{TOT}}{V_{TRAN}}} = \frac{1 + G \cos \phi}{G_{TOT}}$$

From the geometry at a point in the vortex wind field or grid, $\phi = P + \beta + \frac{\pi}{2}$. For a given vortex, $V(r)$ and $\beta(r)$ must be specified in order that wind fields can be generated. Then at each point (r, P) measured from the vortex center and counterclockwise from the direction of V_{TRAN} , ϕ is determined. For a range of V_{TRAN} , $G(r)$ will be specified and thus G_{TOT} and ψ may be calculated. Dimensional values of the wind speeds may be recovered through multiplication by V_{TRAN} .

A choice arises in fixing the scale of flow or grid size for the Rankine-like vortex wind field. Depending on the resolution of the vortex flow desired, calculations can be carried out on a rectangular grid which has 900 grid points. In this study the solid rotation grid size represents the most resolution and shows in detail the velocities inside the radius of maximum wind. The potential flow grid, however, represents the scale of flow where the maximum resolution occurs for the region outside the radius of maximum wind. The Rankine flow is an overall view of the two previous flows but with less resolution than either of them.

The Rankine-type flow is characterized by solid rotation from the center of the vortex or flow field out to a radius where the maximum velocity for a stationary vortex occurs. Beyond this radius, potential flow is established. For solid rotation the rotational velocity increases linearly from zero at the origin to the radius where the rotational velocity is a maximum. Non-linear increases may be used, such as r^2 or r^3 , but they were not chosen for this particular study.

(Limited evidence from actual vortices suggests the linear dependence is satisfactory.) The potential flow beyond the radius of maximum rotational velocity is characterized by a rotational velocity inversely proportional to the radius; therefore, the rotational velocity decreases with the increasing radius as $1/r$. The Rankine-type flow then permits an over-all view of the vortex with 32 of the 900 grid points representing the solid rotation while the remaining 868 points represent the potential flow.

Another choice for grid representation may be termed "solid rotation." In this grid 675 of the 900 grid points are within the region of solid rotation while the remaining 225 points are in the potential flow. The solid rotation scale yields a detailed picture of the inner portion of the vortex.

The third grid choice is called the "Potential flow grid." In this grid only four points represent the solid rotation with the remaining 896 points displaying the potential flow. This scale simulates the flow patterns at large distances away from the vortex center.

These scales for depicting the vortex are not chosen without reason. In the case of the solid rotation scale, the structure of the innermost portion of the vortex may be investigated. The potential flow scale brings to attention broad-scale features or features that remain nearly uniform at large distances. The Rankine-type scale is used as an intermediate scale and is the scale most beneficial because of its capacities of combining the most interesting features of both the other scales. It should be noted that any scale could be used for computation by simply changing a single parameter in the computer program.

After establishing the grid sizes for the different flow fields, there are several necessary idealizations for a moving vortex. In order to investigate complex swath patterns generated by an actual translating tornado, simplifications must be imposed in order that general characteristics may be recognized in the numerically-generated swath patterns. After the general characteristics have been elucidated, investigators of tornado damage may be able to better interpret damage

patterns in terms of the tornado wind structure.

In order that general characteristics can be deduced from generated swath patterns the following assumptions are imposed:

1. Uniformly spaced objects are in the path of the tornado. (For convenience, these objects are referred to as trees.)
2. Each tree has a critical wind speed value for failure.
3. When this critical value for failure is reached or exceeded, the tree falls at the angle of the wind that causes the tree to fall.
4. Winds of less than the critical speed have no effect on the tree.
5. Once the tree fails and falls, it remains in that position even though higher winds at different angles might be reached later.
6. No interaction is allowed between trees.

The velocity at which an object will fail (V_{CRIT}) may have any specified positive value. G_{CRIT} , defined as V_{CRIT}/V_{TRAN} , is a dimensionless quantity; i.e. if $G_{CRIT} = 4.0$ and V_{TRAN} was specified as 20 m/sec, V_{CRIT} would be equal to 80 m/sec. The non-dimensional quantity, G_{CRIT} , is used in order to readily obtain V_{CRIT} for many translational velocities.

It is of interest to obtain swath characteristics not only for an unchanging vortex but also for a tornado in evolution. Swath characteristics produced by a steady-state vortex are generated by assuming a uniform G_{CRIT} across the tornado and simulating the passage over several rows of trees. For the evolving tornado, the particular swath characteristics depend on the chosen evolutionary sequence of the tornado wind field; theoretical and observational studies suggest several possibilities. An example of a damage track for an evolving tornado from formation to dissipation may be illustrated by combining successive tornado swath patterns into one long, simulated path.

CHAPTER IV

METHOD OF SOLUTION

In order to generate the wind field for a particular vortex, the velocities (magnitudes and directions) at particular points (radius from the center of the vortex and angle measured counterclockwise from the direction of translation) are calculated. First, the scale of the vortex is specified; the scale of flow is very important because of the detail required at different points in the vortex. As mentioned earlier the greatest detail is available when the solid rotation flow scale is used. To obtain an overview of the entire vortex structure, the potential flow scale is utilized.

Once the scale of motion for a particular vortex is specified the next step is to determine the position of the grid point with respect to the vortex center. The position of the point yields an angle with respect to the translational motion and the distance from the vortex center (i.e. similar to polar coordinates). The angle obtained is in the range from +180 degrees to -180 degrees with 0 degrees being in the direction of straight line translational flow. A positive degree represents an angle counterclockwise from the translational flow. For a given scale of flow and distance at which the grid points are located from the vortex center, the proper equation would be used to calculate the rotational velocity depending on whether the point is within the solid rotational or potential flow region.

The angle of inflow (β) is a very crucial parameter for the vortex wind field. It is defined as the angle between the rotational velocity and the tangential velocity. Listed below are the critical regions for β :

$\beta = -90^\circ$	outflow
$-180^\circ < \beta < -90^\circ$	divergence (anticyclonic)
$\beta = -180^\circ$	clockwise rotation
$90^\circ < \beta < 180^\circ$	convergence (Southern Hemisphere cyclonic)

- $\beta = 90^\circ$ inflow
- $0 < \beta < 90^\circ$ convergence (cyclonic)
- $\beta = 0^\circ$ counterclockwise rotation
- $-90^\circ < \beta < 0^\circ$ divergence (S.H. anticyclonic)

If the angle of inflow, β , is equal to 0° at a point, pure cyclonic rotation (counterclockwise in the Northern Hemisphere) exists. As β decreases below 0° , the flow becomes different until $\beta = -90^\circ$. With $\beta = -90^\circ$ pure outflow is represented. An anticyclonic (clockwise) tornado is represented by $\beta = -180^\circ$. While most tornadoes documented in the Northern Hemisphere are cyclonic, some may be anticyclonic (Fujita, 1977a). A more realistic case for the flow for tornadoes in the Northern Hemisphere seems to be for β to be greater than 0° but less than 90° . A good approximation to the inflow angle in most cases is 30° , which is the standard inflow angle established by the U.S. Nuclear Regulatory Commission for design studies.

Other parameters needed to establish a particular vortex include the radius at which the maximum wind occurs and the magnitude of that wind. In the formulation of the problems, the radius at a particular point is non-dimensionalized in terms of the radius of maximum wind (i.e. the radius at a particular point is given in terms of the number of radii from the center to that particular point; one radius was defined as the distance from the center to the radius where the maximum rotational velocity occurs). The radius of maximum wind for the vortex is located at $r = 1$. A radius of two is at a distance two times the radius from the vortex center. Dimensionalizing the radius is accomplished by a simple multiplication of a dimensional quantity (i.e. if $r = 1$ is really at a radius of 50 meters, then all r values are multiplied by 50 m to recover the actual radii).

With the maximum wind (V_{MAX}) known or given a new parameter $G_{MAX} = V_{MAX} / V_{TRAN}$ can be defined and used in the computer program. In this way specification of different G_{MAX} 's leads to the output for wind fields corresponding to the same general vortex being translated at different translational speeds. The range of nondimensional G_{MAX}

values used is 0.5, 1, 4, 6, 10, 20, 50, and 130. If V_{MAX} for a particular vortex is 100 m/sec, the corresponding V_{TRAN} 's are 200, 100, 25, 16.67, 10, 5, 2, and 0.77 m/sec, respectively.

Once the wind field is generated for a particular vortex, numerically simulated swath diagrams are formulated. The numerical sequence requires that a critical wind speed be reached or exceeded in order that the object fail. In all cases it is assumed that the critical speed (G_{CRIT}) be uniform across the width of the tornado path and that the objects are uniformly spaced. Each swath generated has a possibility of 30 objects being downed. In a few cases the G_{CRIT} is uniform across the breadth of the tornado track but is changing with respect to the length indicating what might be the evolution of a tornado. For example, the tornado might begin as a weak vortex then transform to a strong vortex with dissipation occurring later in its life cycle. This evolution process is simulated by using a typical G_{CRIT} value of 1 increasing gradually to 4 with a reduction again to 1 or 0, while V_{TRAN} is considered to remain constant. Any number of combinations may be used for this simulation.

Previously, reference has been made to a translational velocity oriented uniformly across the vortex with the direction of translation for the vortex parallel to the translational velocity itself. Questions arise: What is the effect of a translational shear and/or curvature on the basic flow pattern of the vortex? Furthermore, can the wind field of a tornado with multiple vortices be simulated in a simple way using the technique for shear and/or curvature together with the original vortex? With many simplifying assumptions, it has been possible to simulate such cases.

CHAPTER V

RESULTS AND DISCUSSION

The investigation of simulated tornado wind fields reveals locations where the magnitude of the wind velocity attains maxima and minima. The areas of minimum velocity (calm) generally occur in either the left forward or left rear quadrant of a cyclonic vortex (looking in the direction of translation which is the top of the figure). With respect to a vertical line and a horizontal line extending through the vortex center, the quadrants are labeled left or right and forward or rear, respectively. The location of the calm depends primarily on the angle of inflow and the strength of the vortex. For a weak vortex with $G_{MAX} < 1$ (i.e. the translational speed is greater than the rotational speed) the speed does not decrease to zero. For $G_{MAX} = 1$, however, a calm or stagnation point does exist on the radius of maximum rotational speed and to the left of the center of the vortex. In the figures the "+" denotes the vortex center. Also in the figures the "X" represents a point of maximum wind. Depending upon the direction of radial flow (inflow or outflow) the stagnation point will either lie in the left forward or rear quadrants. For inflow ($\beta > 0^\circ$) the location is the left forward quadrant; for outflow ($\beta < 0^\circ$) the location moves to the left rear quadrant.

Isotach (line of constant V) and streamline patterns are constructed from a thirty by thirty array of point values V_{TOT} and ψ . The method used for constructing streamlines follows Sandström's (1909) procedure. Both the isotachs and streamlines reveal characteristic features in the wind field patterns.

The Rankine vortex provides the fundamental distribution of winds used in comparing the net effects of vortex structures. A dimensionless formulation, wherein all speeds are scaled by V_{TRAN} , is adopted, for which the maximum velocity occurs at $r = 1$. As defined earlier,

within $r = 1$ the speed increases linearly with the radius; outside $r = 1$, it decreases with the inverse of the radius. Letzmann called these two regions the core and the mantle, respectively. Combining the study of the vortex structure on three grid size representations (solid rotation, Rankine vortex, and potential flow) brings out the most important features of the vortex. Solid rotation can represent either a closeup view of the core inside the Rankine vortex or it can illustrate a vortex that consists almost entirely of solid rotation. The potential flow, however, may represent a vortex on a large-scale or a vortex with a small core, consisting mostly of the mantle.

Wind Fields

The isotach pattern shows a family of circles enclosing the inner calm point along with a family of crescents for the range of $G = G_{MAX} \pm 1$ enclosing the area of maximum wind. (In theory the tips of the crescents should be pointed, but since calculations were not sufficiently dense, round tips are depicted.)

Different patterns of isotachs and streamlines are governed by the parameters G_{MAX} and β . Changes in these two parameters are illustrated in the next several figures. In Fig. 2, a Rankine vortex is illustrated with $G_{MAX} = 1$ and $\beta = 30^\circ$. With this example there exists a calm point located on the radius of maximum rotation along with the maximum velocity on the same radius from the center. If G_{MAX} is increased to $G_{MAX} = 4$, two calm points appear - one inside r_{MAX} and one outside r_{MAX} . This is illustrated by Fig. 3 with $G_{MAX} = 4$ and $\beta = 30^\circ$. If, however, G_{MAX} increases further (Fig. 4) the internal calm approaches the vortex center while the external calm moves to a larger radial distance.

The inflow angle β also plays an important role in establishing the location of the calm points. For example, with $\beta = 0^\circ$ (no inflow, pure cyclonic rotation), the calm point is found directly to the left of the vortex center (Fig. 5). With $\beta = -30^\circ$ (indicating a vortex with

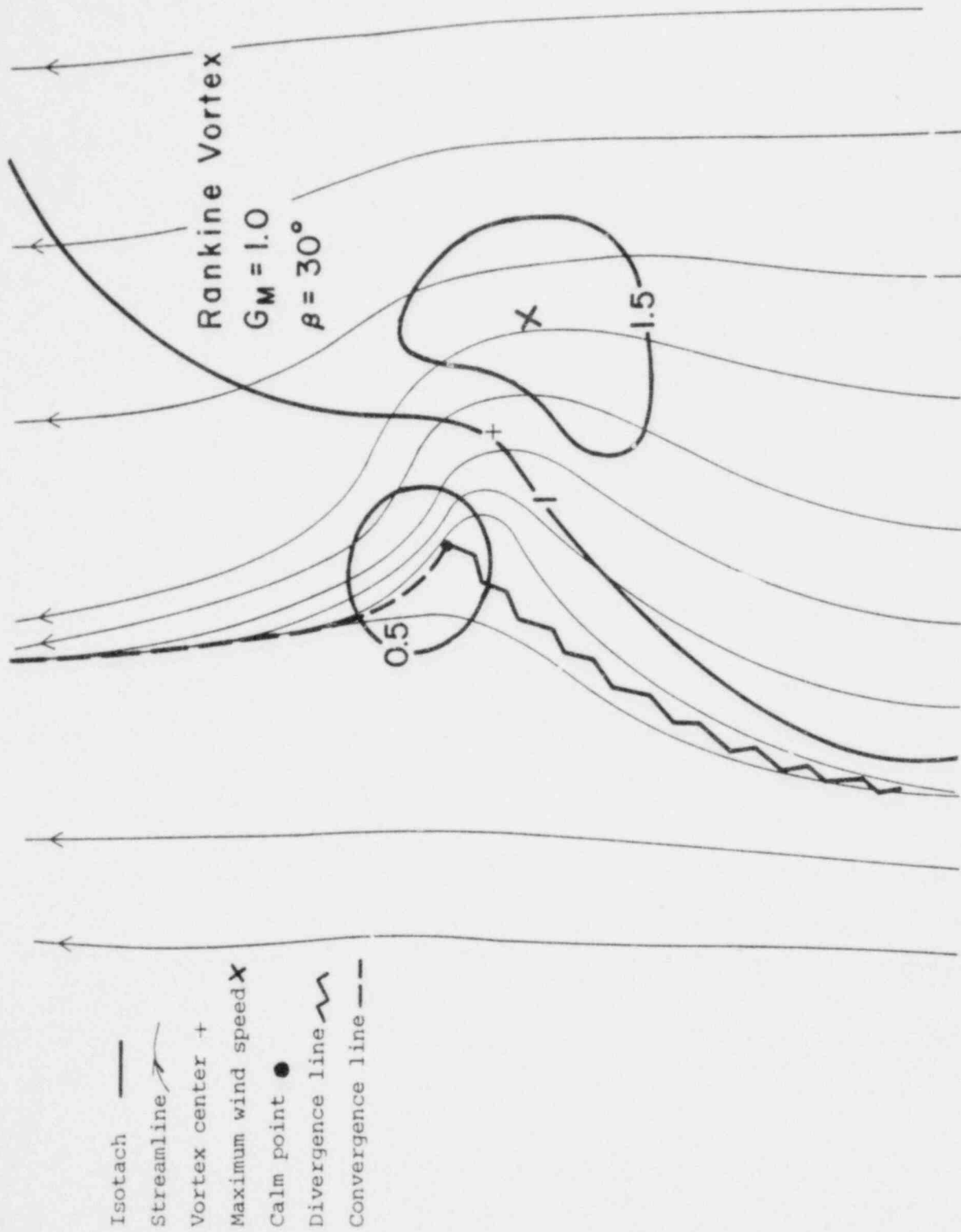


Fig. 2. Isotachs and streamlines for $G_{MAX} = 1$ and $\beta = 30^\circ$ for a Rankine vortex.

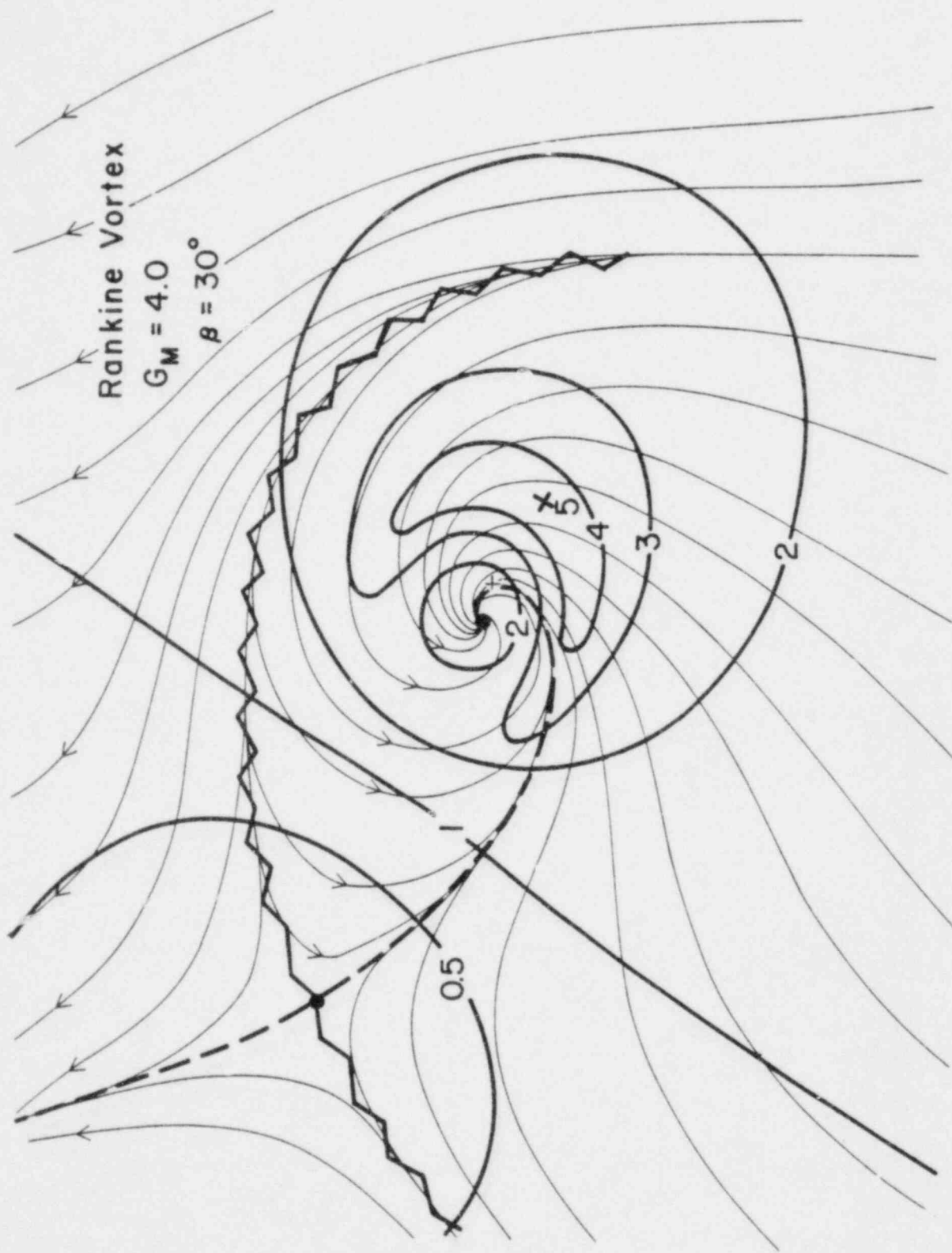


Fig. 3. Isotachs and streamlines for $G_{MAX} = 4$ and $\beta = 30^\circ$ for a Rankine vortex.

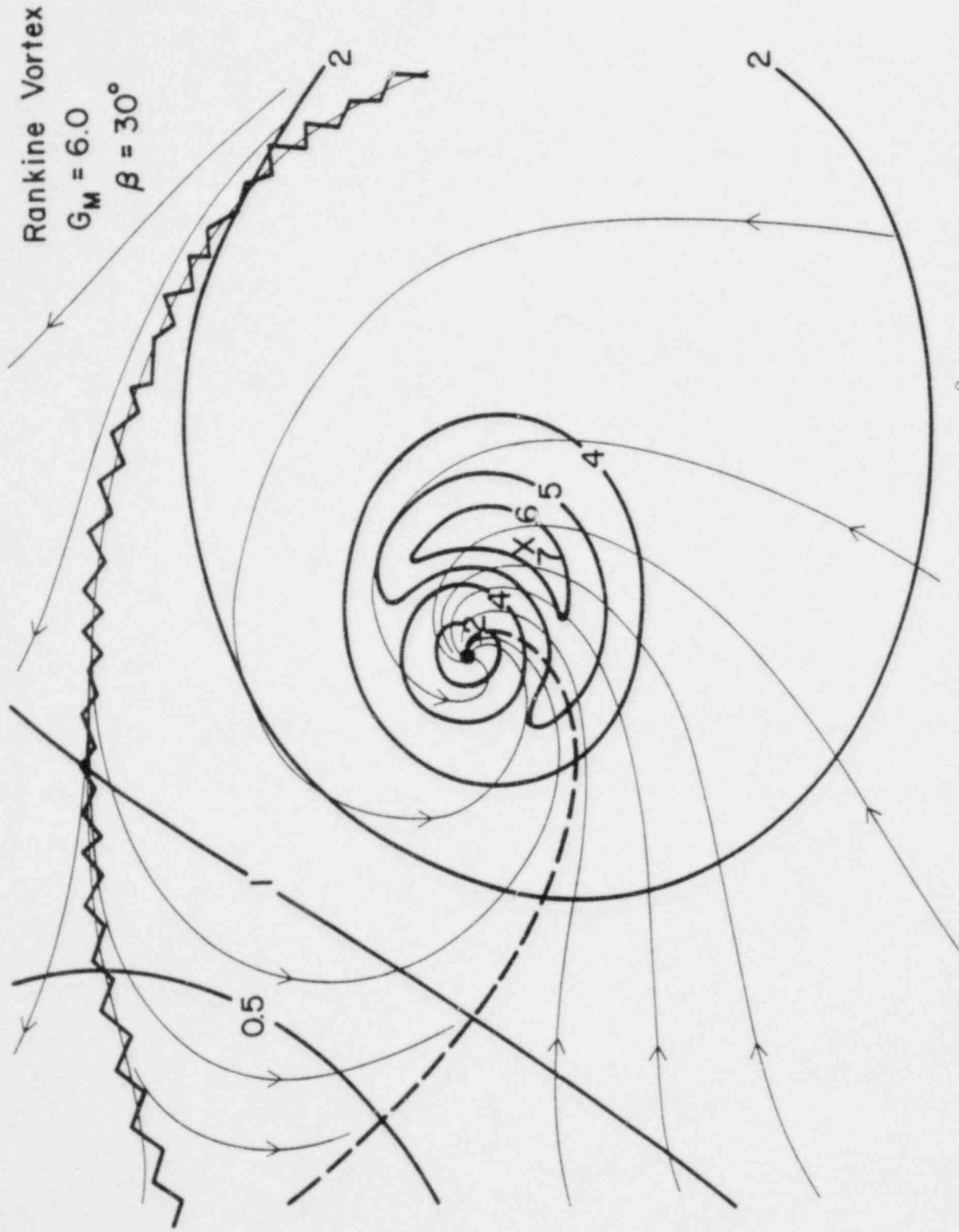


Fig. 4. Isotachs and streamlines for $G_{MAX} = 6$ and $\beta = 30^\circ$ for a Rankine vortex.

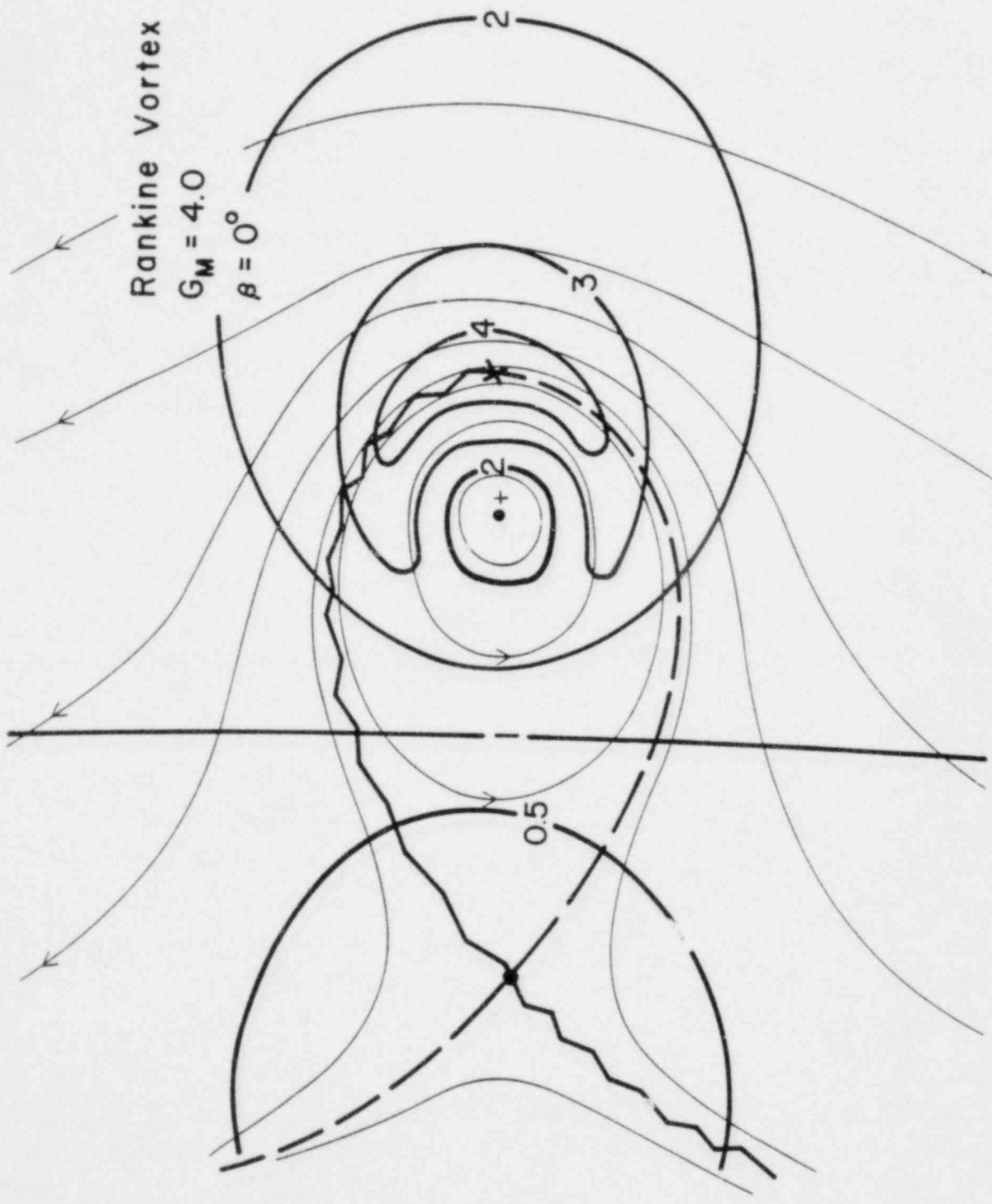


Fig. 5. Isotachs and streamlines for $G_{MAX} = 4$ and $\beta = 0^\circ$ for a Rankine vortex.

outflow) the calm points occur in the left rear quadrant (Fig. 6). If $G_{MAX} = 4$ and $\beta = 60^\circ$ (Fig. 7) the structure is similar to Fig. 5 only rotated 60° clockwise. For the case of pure inflow $\beta = 90^\circ$, illustrated in Fig. 8, the stagnation points are located directly ahead of the center of the vortex.

If the vortex existed with internal outflow ($\beta < 0$) and external inflow ($\beta > 0$) relative to the radius of maximum wind the calm points would not lie along the same azimuth. The calm point of the internal region is found in the left rear quadrant, while the calm point for the external region is located in the left forward quadrant.

A broader region of relative calm within the vortex may be defined where $|V_{TOT}| < |V_{TRAN}|$. For small values of G_{MAX} , however, the percentage of this total calm area decreases. This was portrayed by Letzmann (1924) and is shown in Fig. 9 for a given vortex.

Examination of the streamlines for the Rankine vortex reveals two additional features; a convergence line (---) and a divergence line (\wedge). For example, in Fig. 3, the streamline pattern illustrates the presence of the convergence and divergence lines. The convergence line forms on the left side of the vortex and consists of two parts. One section of this line, from the outer calm curving inward into the inner calm, may be thought of as a line representing the air converging into the vortex center. The upper section of this line, upward from the outer calm, is the location of a weaker converging current that does not enter the vortex core. The divergence line in general represents a separation between the air flowing into the vortex center and the air not reaching the center. The same vortex is shown from a broader perspective in Fig. 10.

For the no inflow case ($\beta = 0^\circ$) shown in Fig. 5, the wind field pattern is to some extent symmetric with respect to the line perpendicular to the translational direction (referred to as "horizontal" later) through the vortex center. As the inflow angle increases, this line begins to tilt toward the forward left quadrant (Fig. 3). At $\beta = 90^\circ$ (Fig. 8) there is true symmetry and the line becomes vertical.

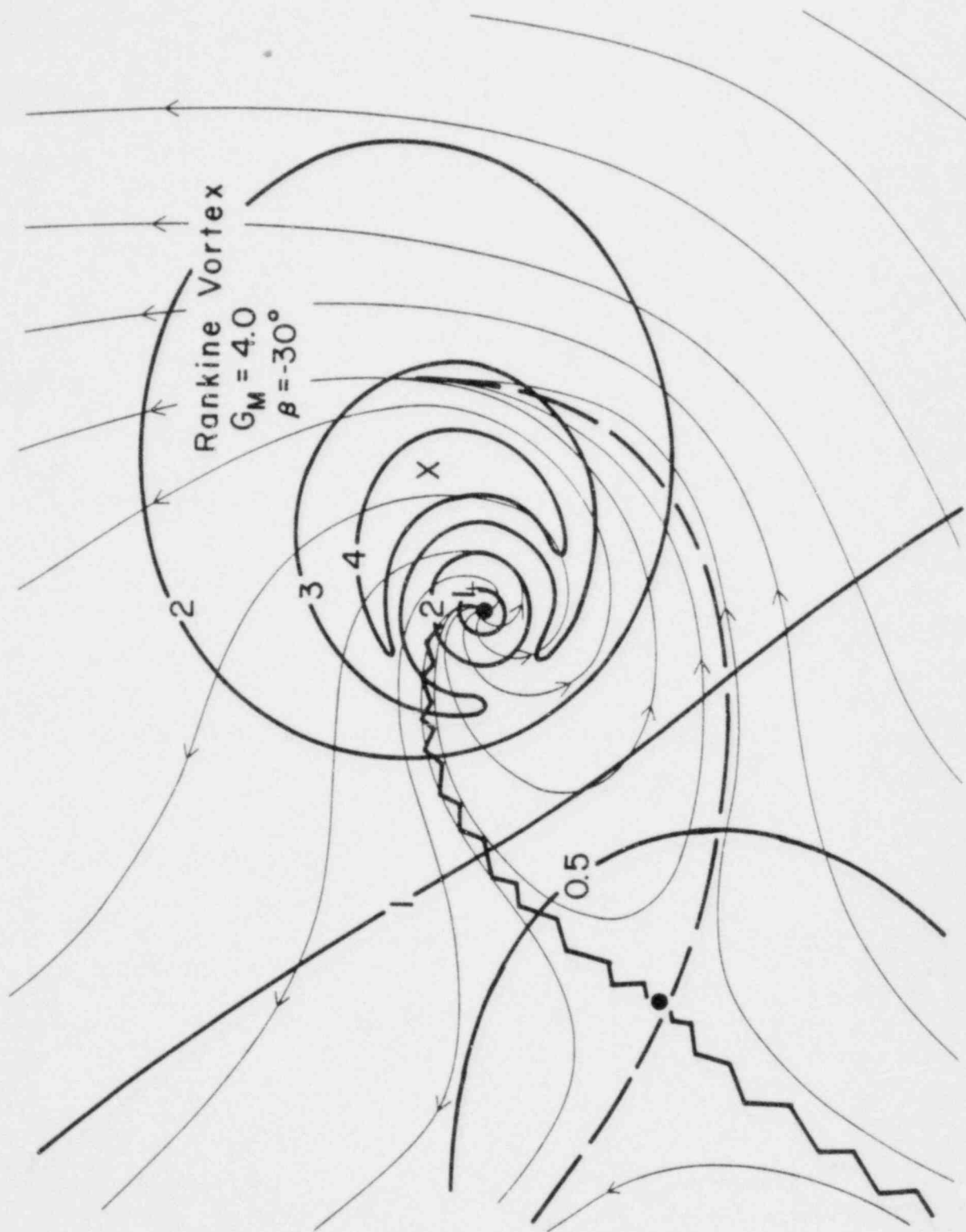


Fig. 6. Isotachs and streamlines for $G_{MAX} = 4$ and $\beta = -30^\circ$ for a Rankine vortex.

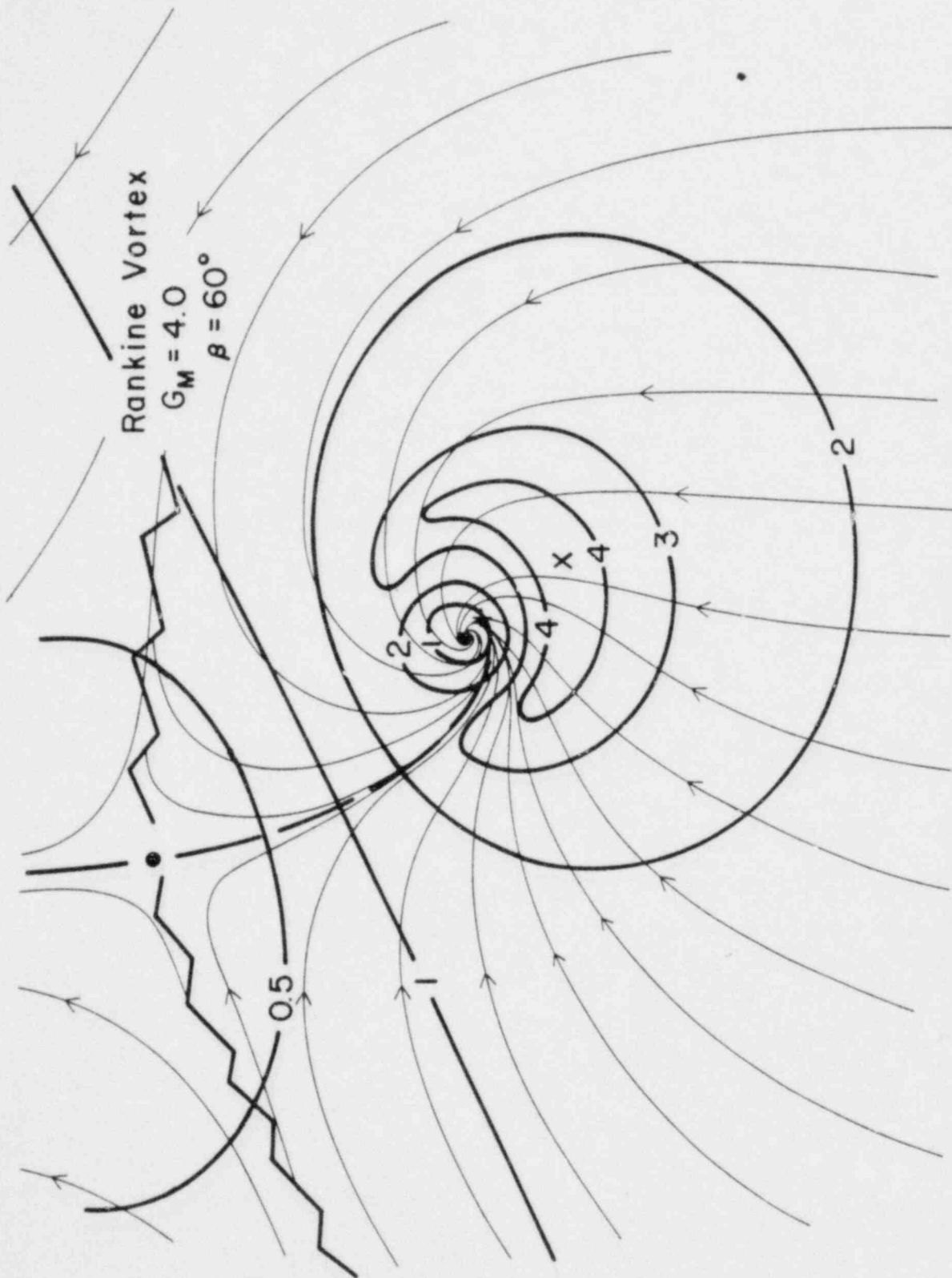


Fig. 7. Isotachs and streamlines for $G_{MAX} = 4$ and $\beta = 60^\circ$ for a Rankine vortex.

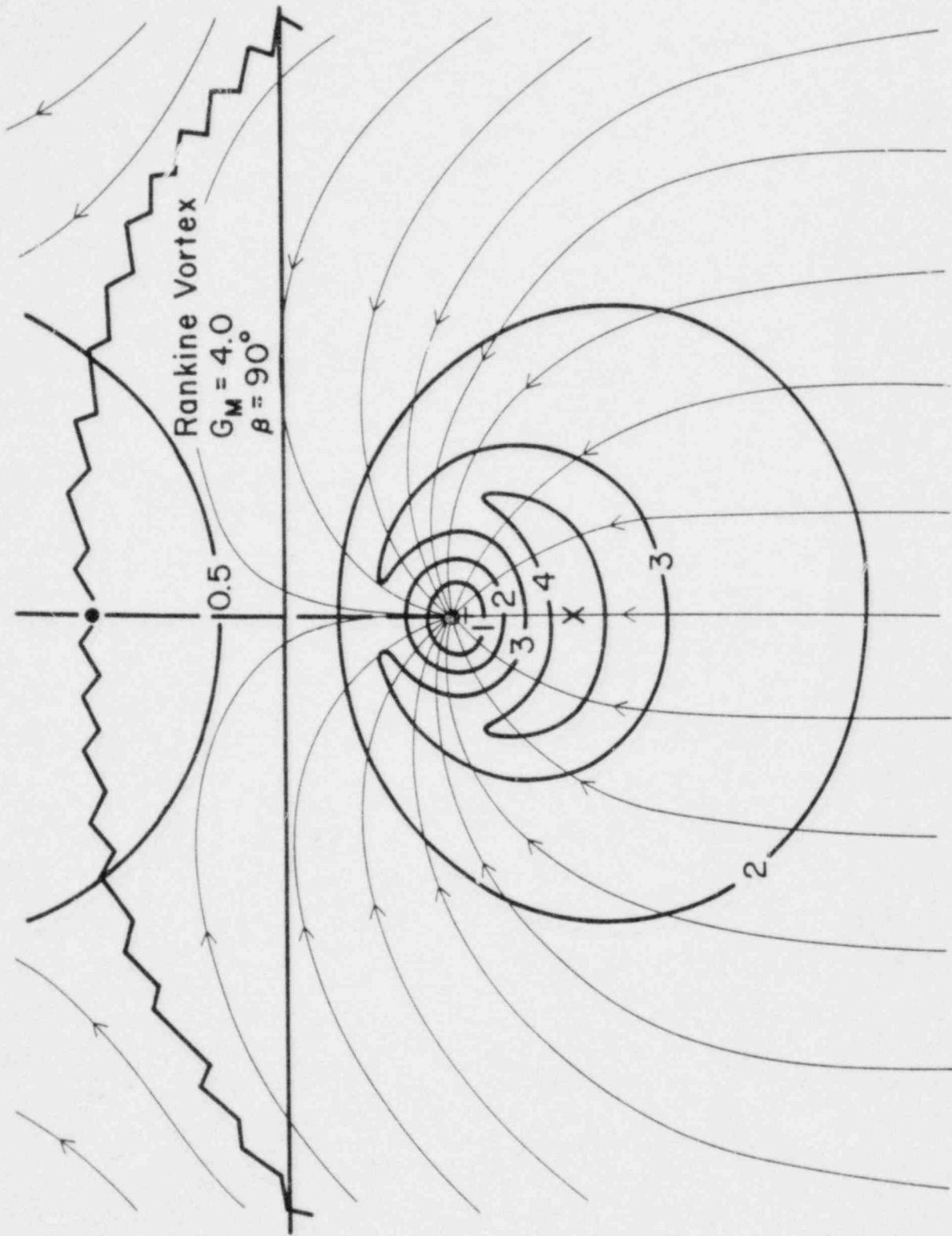


Fig. 8. Isotachs and streamlines for $G_{MAX} = 4$ and $\beta = 90^\circ$ for a Rankine vortex.

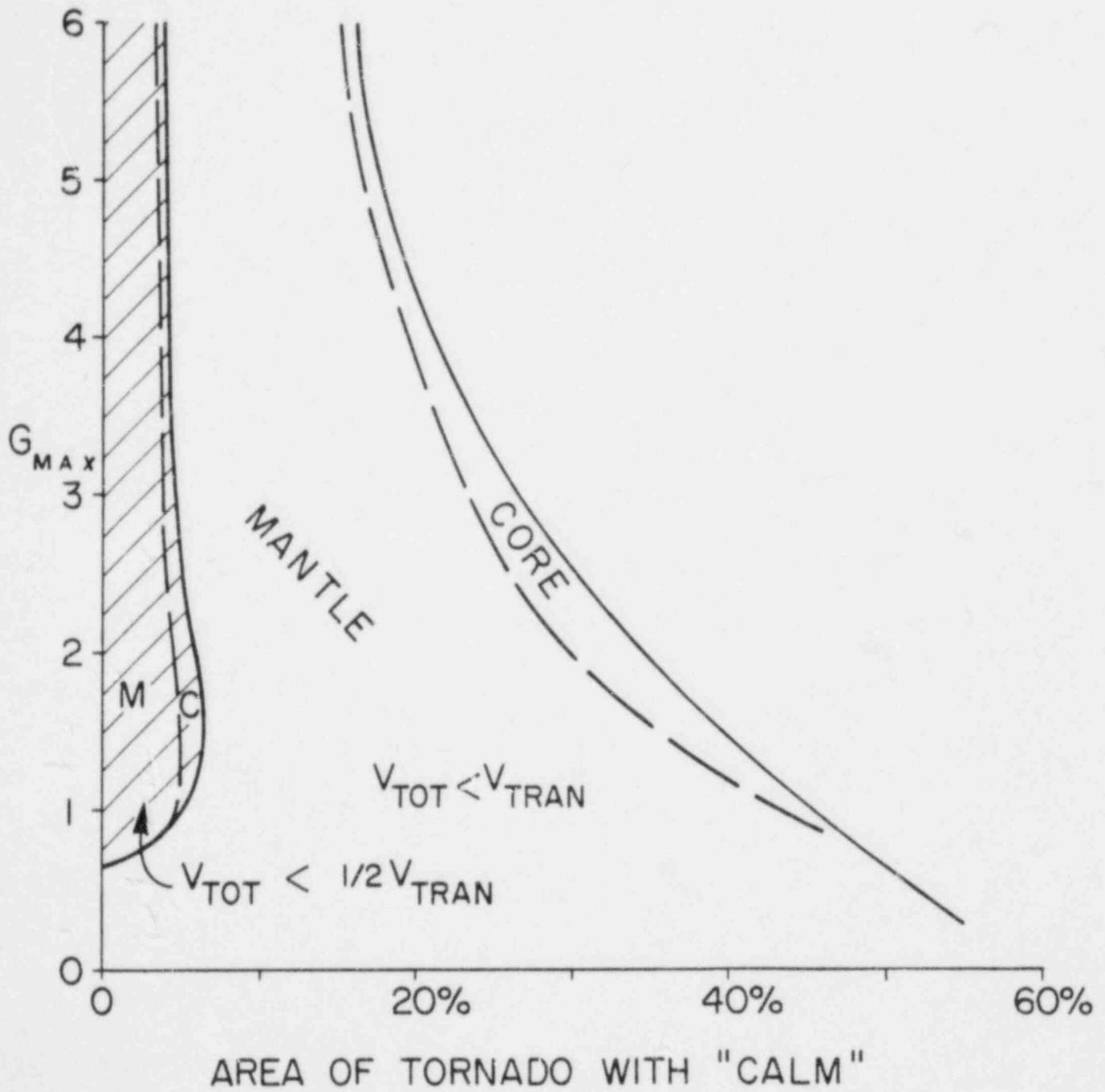


Fig. 9. Percentage of the vortex field experiencing relative calm, $|v_{TOT}| < |v_{TRAN}|$ (after Letzmann, 1924).

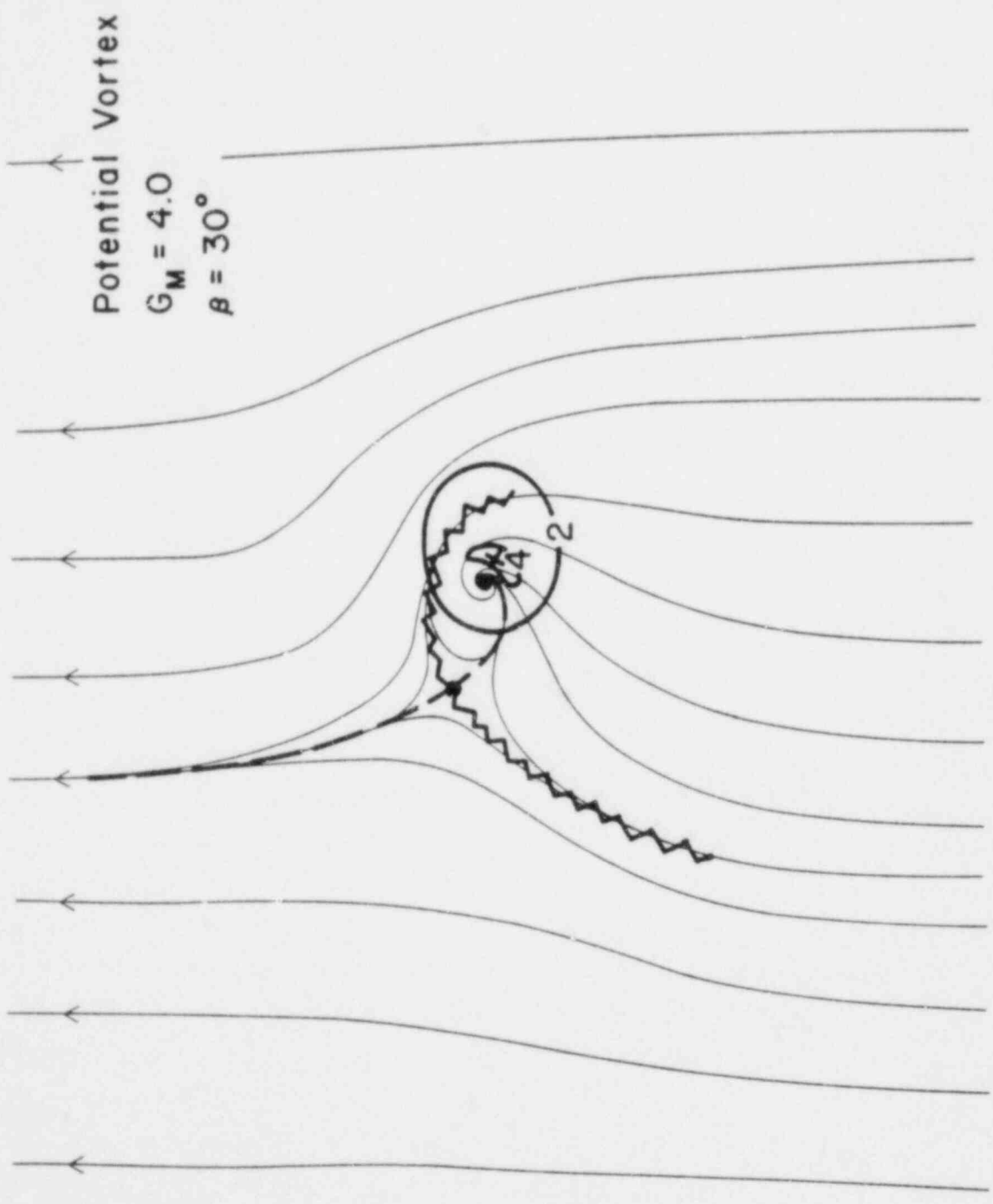


Fig. 10. Isotachs and streamlines for $G_{MAX} = 4$ and $\beta = 30^\circ$ for a potential vortex.

In general as G_{MAX} increases, the patterns of streamlines remain generally the same but more intense. The calm point positions do separate, however, with the interior calm approaching the vortex center and the external calm moving out to greater distances. For a smaller G_{MAX} , the streamline pattern weakens and a transformation occurs. The calm points merge to a point which is at the radius of maximum winds, as illustrated in Fig. 2. Also for this case, the convergence and divergence lines have virtually disappeared; furthermore, there exists no flow counter to the direction of translation near and around the vortex center. As G_{MAX} becomes less than one (Fig. 11), the flow is essentially rectilinear perturbed by a very weak circulation. This could be compared to a weak whirlwind with a rapid translational speed.

The importance of the inflow angle is illustrated for a two-cell vortex by Fig. 12. Cyclonic outflow is characteristic in the core of the two-cell vortex. Pure circular flow exists on the radius of maximum winds while pure inflow might exist at large distances from the center. Although not shown, the isogon (and thus the streamline) pattern is not greatly changed from the prototype Rankine vortex.

The previous discussion of wind fields has been based entirely on pure rectilinear (straight) translational motion of the vortex. However, it is observed that tornadoes do not always follow a straight path during their lifetimes. Several non-rectilinear patterns of translational motions have been investigated in an attempt to simulate these realistic motions of tornadoes.

First to be considered is a pattern of sheared flow, for which there is an increase (or decrease) of the environmental wind across the breadth of the vortex. Fig. 13 illustrates the case with a shear of 45 degrees in the flow field of a Rankine vortex. In all cases the value of the shear at the center of the vortex is set equal to unity. A positive shear implies that the increase in velocity is from left to right across the width of the vortex. The angle of the shear is measured from the "horizontal" (as was defined earlier). From this angle a point along the horizontal center line can be found where the

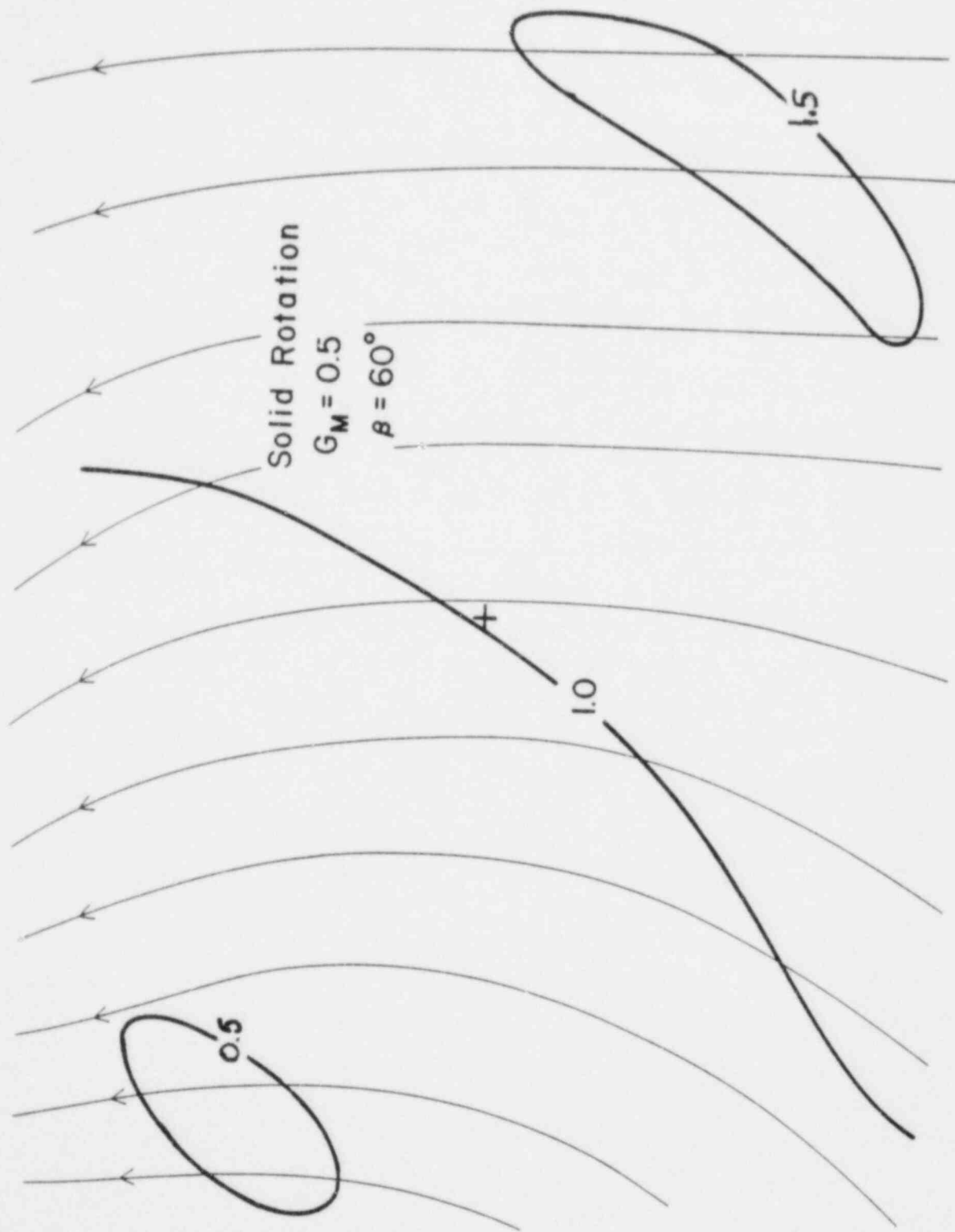


Fig. 11. Isotachs and streamlines for $G_{MAX} = 0.5$ and $\beta = 60^\circ$ for a solid rotation core.

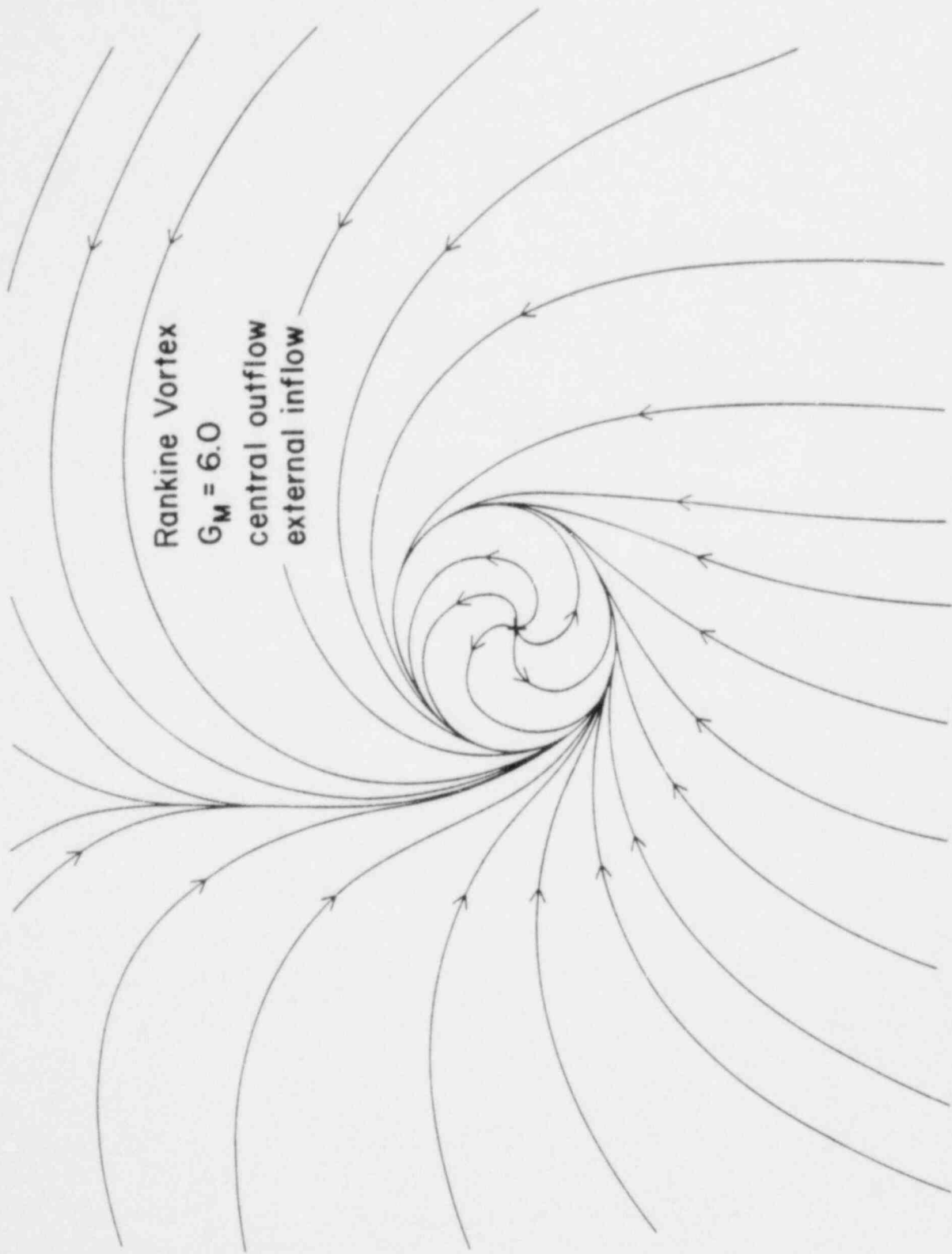


Fig. 12. Streamlines for a Rankine-like, two-cell vortex in translation.

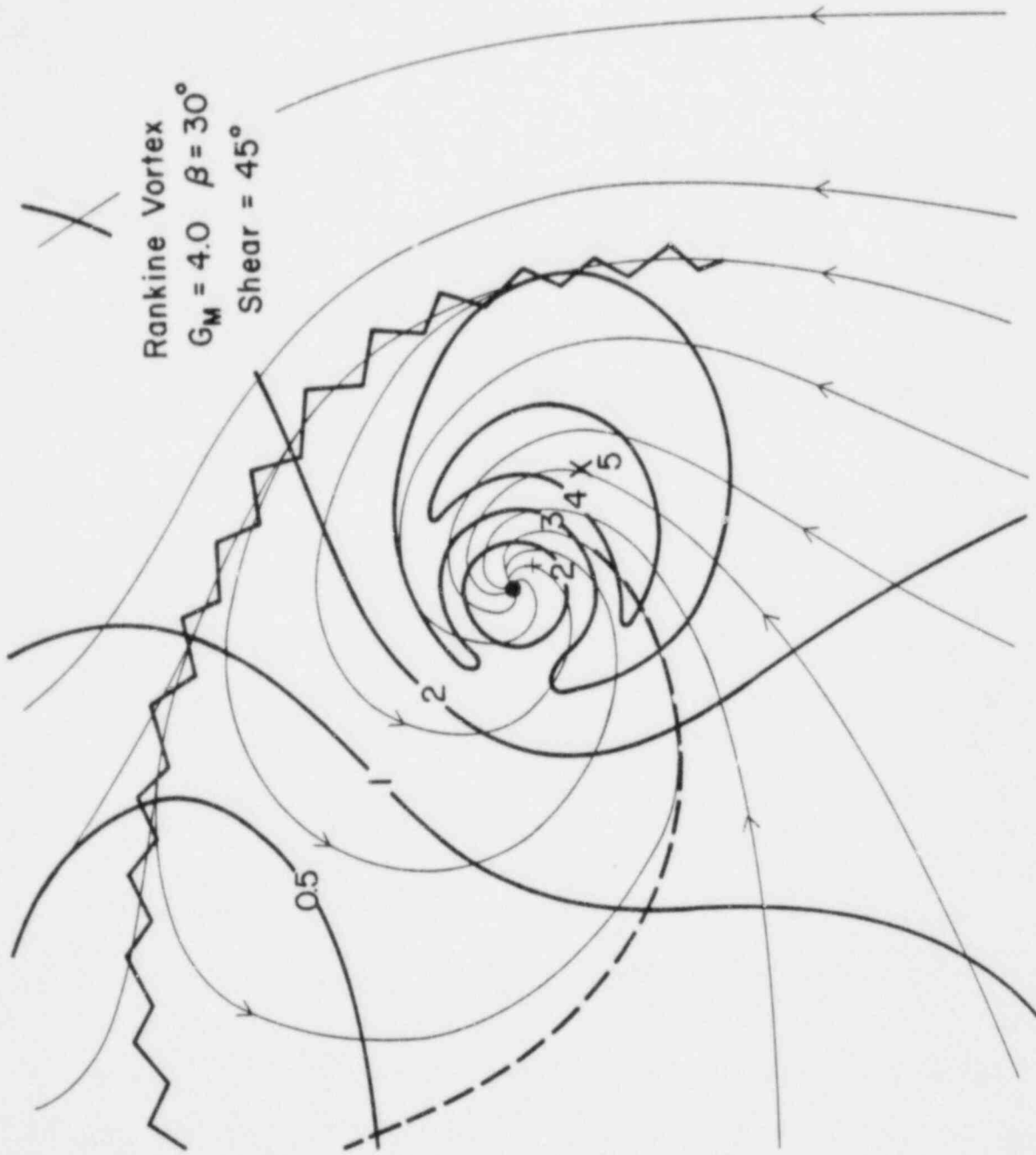


Fig. 13. Isotachs and streamlines for $G_{MAX} = 4$, $\beta = 30^\circ$, and a shear of 45° .

shear is zero. Knowing the distance from the vortex center, where the value of shear is one, to the point where the shear is zero, any value of shear can be computed by simple trigonometry. In terms of the 45 degree shear, the extreme left of the diagram has a shear value of zero and far right has a value of two, both along the horizontal center of the vortex.

Comparison of the no-shear case in Fig. 3 and an extreme case of shear (45 degrees) shown in Fig. 13 reveals noticeable similarities and differences. The maximum velocity and inner minimum velocity occur at almost the same points. As for the no-shear case, the relative magnitudes of their velocities remain constant. However, the outer minimum is shifted further out from the center of the vortex, although along the same azimuth. The most noticeable change occurs in the isotach analysis. The shear plays a significant role in the formation of altered isotach patterns, especially for the 1 and 2 isotachs.

As the shearing angle decreased (Fig. 14), the features become increasingly similar to the no-shear case; the outer calm approaches the original position as does the isotach pattern.

Another possible effect on the translation of a vortex is due to curvature of the translational wind. In order to incorporate curvature into a flow field of a vortex, the center of curvature needs to be established along the horizontal either to the left or right of the vortex center. The center of curvature may lie either to the left (or right) of the vortex center. Its distance Q is given in terms of positive (or negative) multiples of r_{MAX} , the radius of maximum winds. So for $Q = 1$, the center of curvature is located at $1 \cdot r_{MAX}$ to the left of the vortex center; for $Q = -3$ the center of curvature lies to the right a distance $3 \cdot r_{MAX}$ from the vortex center. As the radius of curvature (Q) decreases, the outer calm moves toward the rear of the vortex. Also the calm becomes more distinguishable (as in Fig. 15). Conversely, for larger radius of curvature the wind field becomes increasingly like that for rectilinear motion (as in Fig. 16).

The next step in simulating a non-rectilinear translating vortex

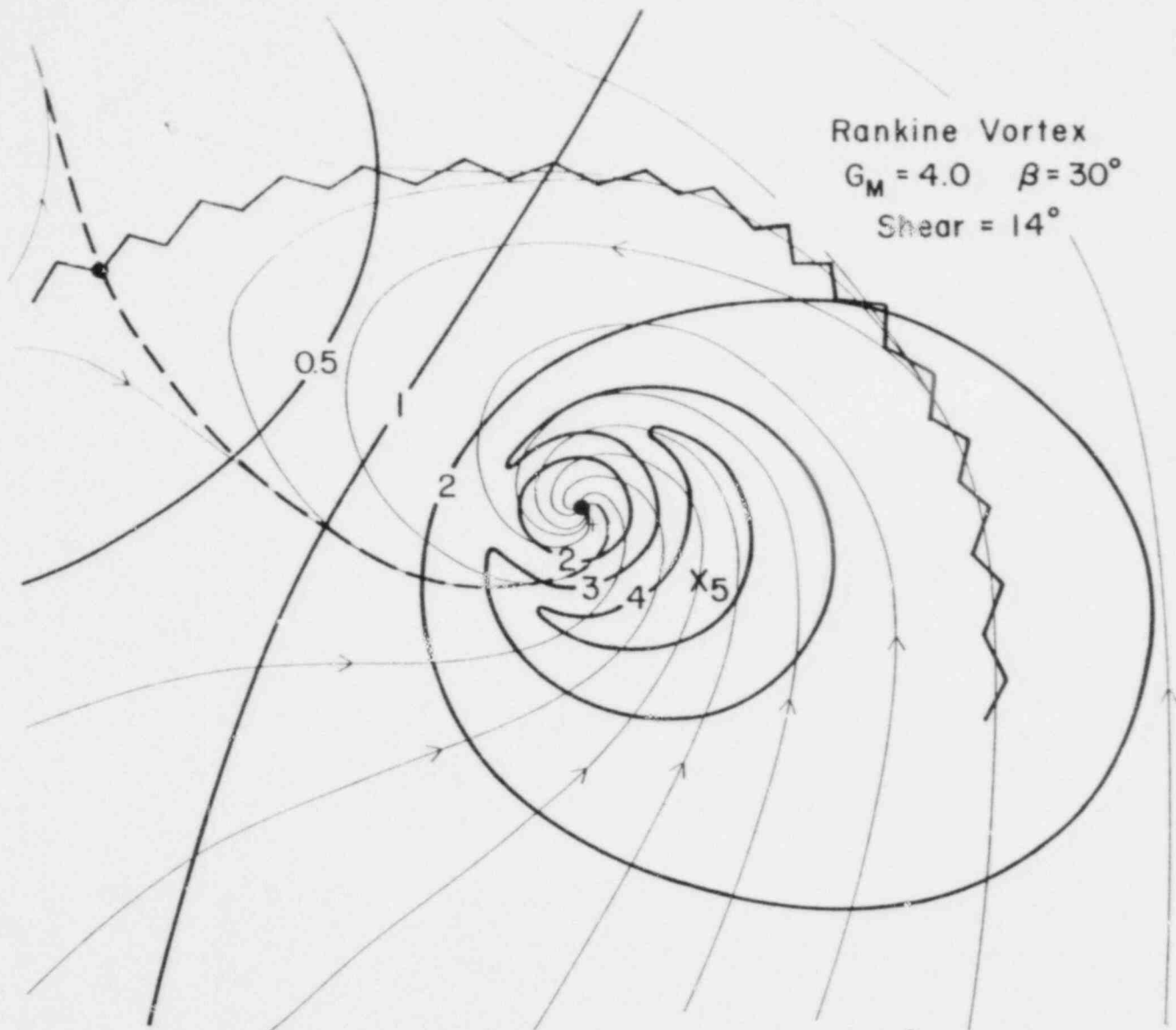


Fig. 14. Isotachs and streamlines for $G_{MAX} = 4$, $\beta = 30^\circ$, and a shear of 14°

Rankine Vortex
 $G_M = 4.0$ $\beta = 30^\circ$
Curvature (Q) = 1.0

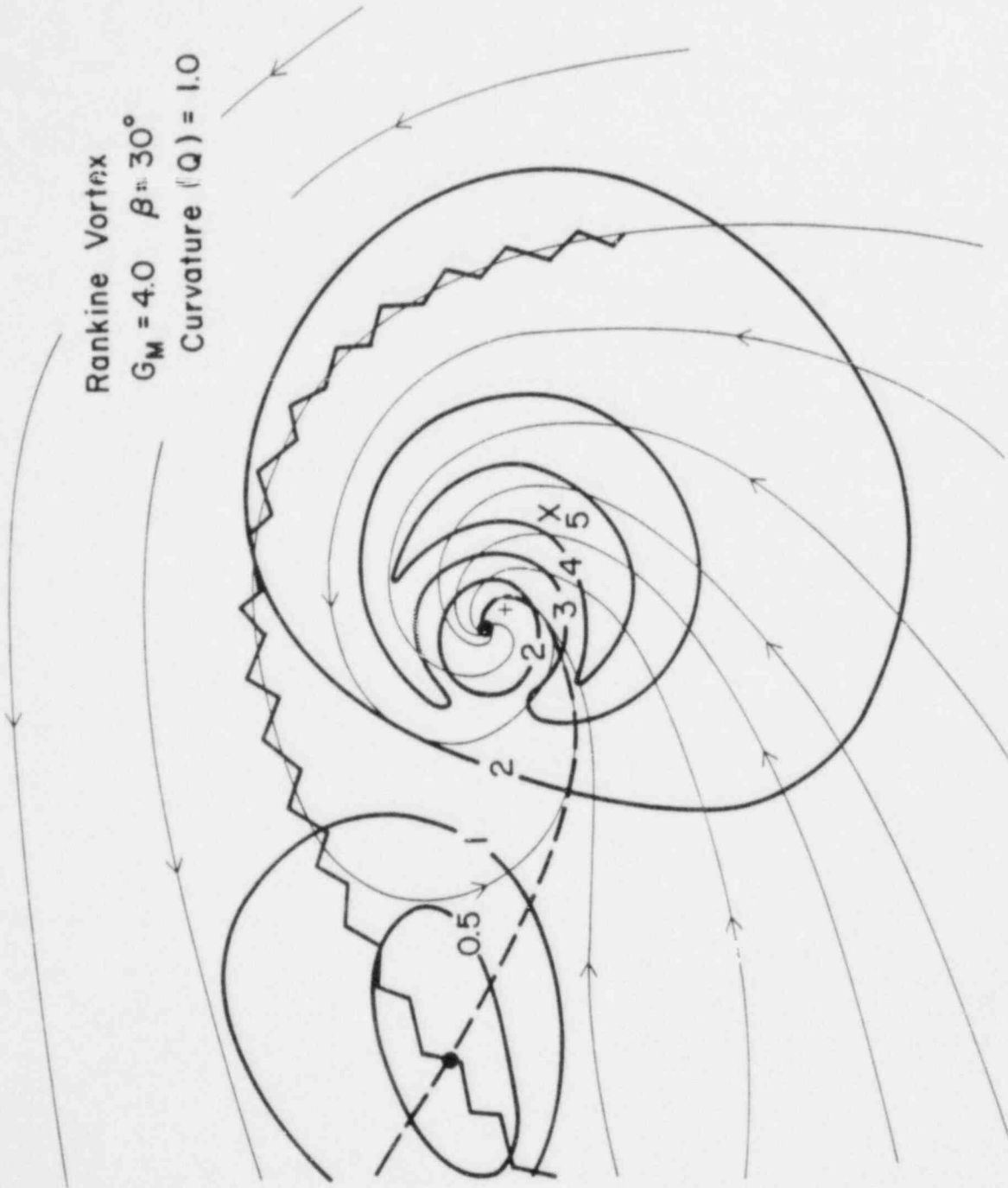


Fig. 15. Isotachs and streamlines for $G_{MAX} = 4$, $\beta = 30^\circ$, and curvature (Q) = 1.

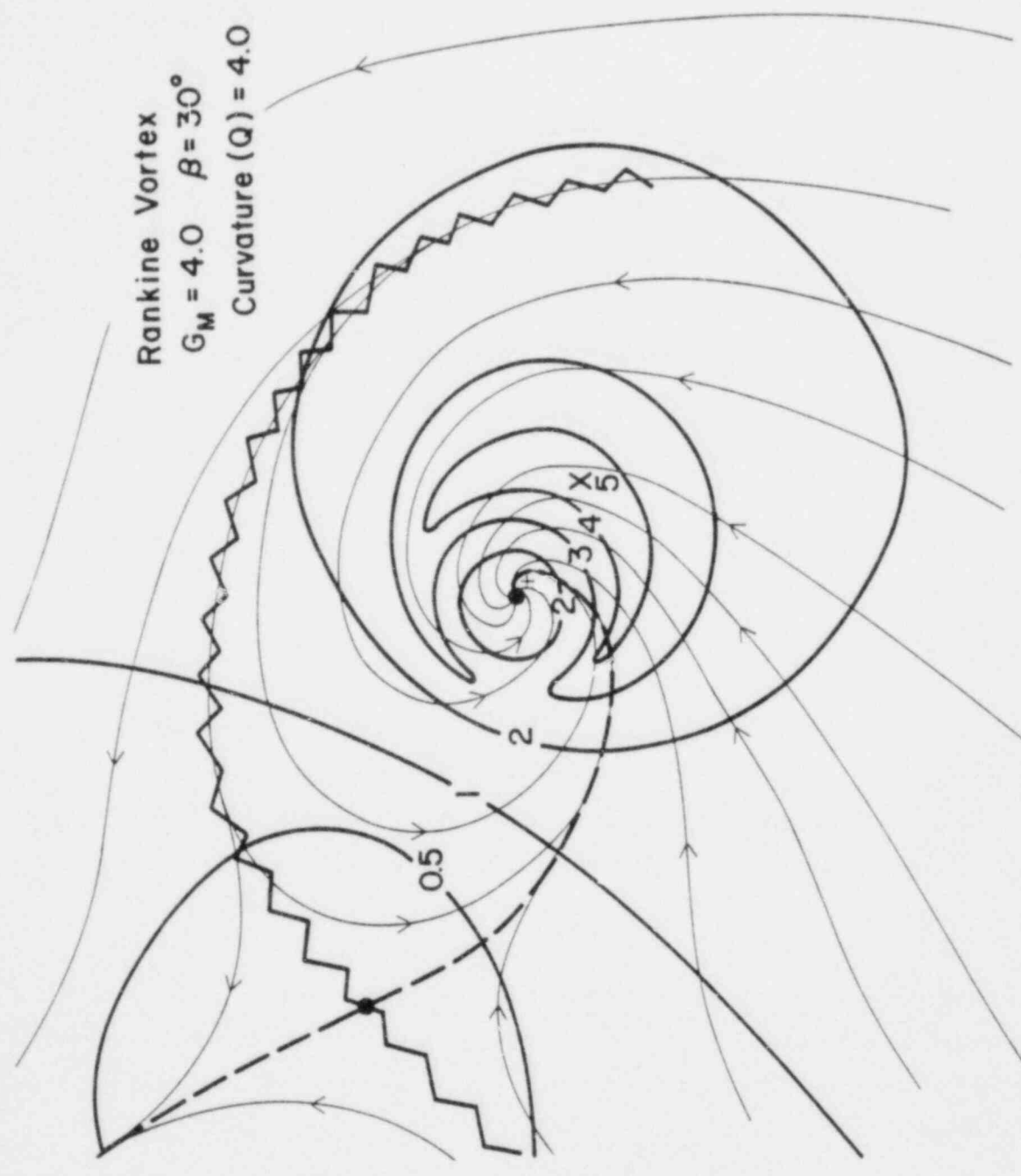


Fig. 16. Isotachs and streamlines for $G_{MAX} = 4$, $\beta = 30^\circ$, and curvature (Q) = 4.

is to combine the shear and curvature features. As before, as the shear is decreased and the point of curvature shifts away from the vortex center (Fig. 17) the rectilinear wind field pattern is recovered. However, with the combination of a 45 degree shear and radius of curvature (Q) equal to 1.0, a new feature arises (Fig. 18). The entire wind field is similar to that of stationary solid rotation; however, the isotach analysis still reveals the presence of the maximum in the right rear quadrant and the inner calm in the left forward quadrant near the vortex center, similar to the case of non-rectilinear translation.

Damage Patterns

Hypothetical damage patterns may be useful in the establishment of tornado characteristics. They are simulated using the computer output for the values of V_{TOT} and ψ . This same output was used previously to construct the streamlines and isotachs. In Chapter III, the assumptions for the creation of swath patterns were presented. These simplifications might seem rather restrictive but they yield reasonable swath characteristics.

One of the simplifications assumes that G_{CRIT} ($\equiv V_{CRIT}/V_{TRAN}$) is uniform across the length and width of the tornado track; another allows no change in the vortex structure. In addition, in order to obtain a swath pattern, scanning of the output begins in advance of the tornado and progresses across the field. Once failure of an object occurs, no other response is allowed as the tornado progresses.

Fig. 19 presents typical damage patterns that might occur for different types of tornado structure. This figure does not in general represent a single complete tornado damage swath. The individual swath patterns are however calculated for cyclonic tornado motion in the Northern Hemisphere with G_{MAX} greater than one. (The objects that have failed will be referred to as "trees" for convenience.)

The simplest case in Fig. 19 is "d" for which $\beta = 0^{\circ}$ (implying no radial motion). The basic pattern for all values of G_{CRIT} suggests divergence. For small G_{CRIT} , cyclonic circulation is shown by the

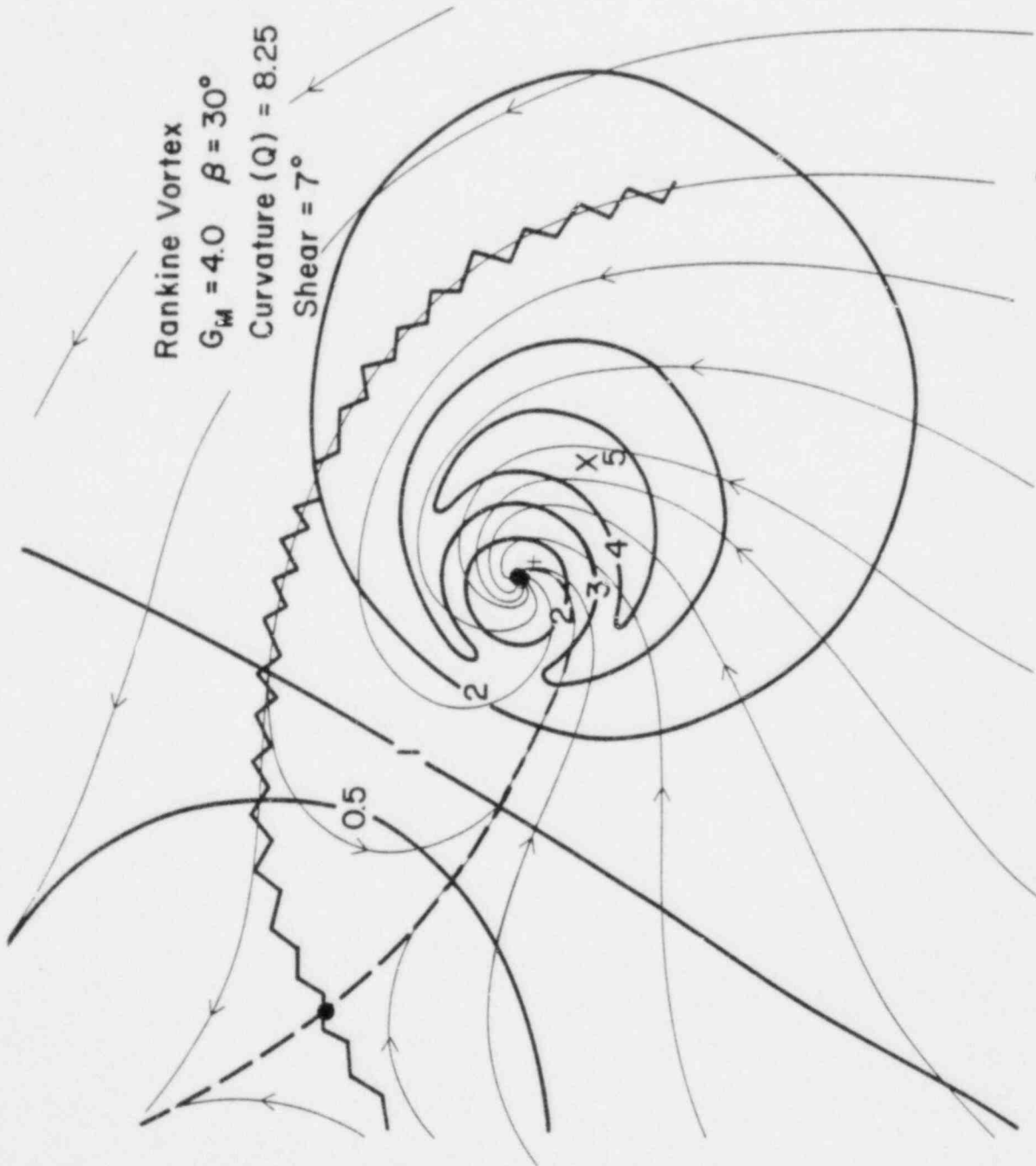


Fig. 17. Isotachs and streamlines for $G_{MAX} = 4$, $\beta = 30^\circ$, shear of 7° , and curvature (Q) = 8.25.

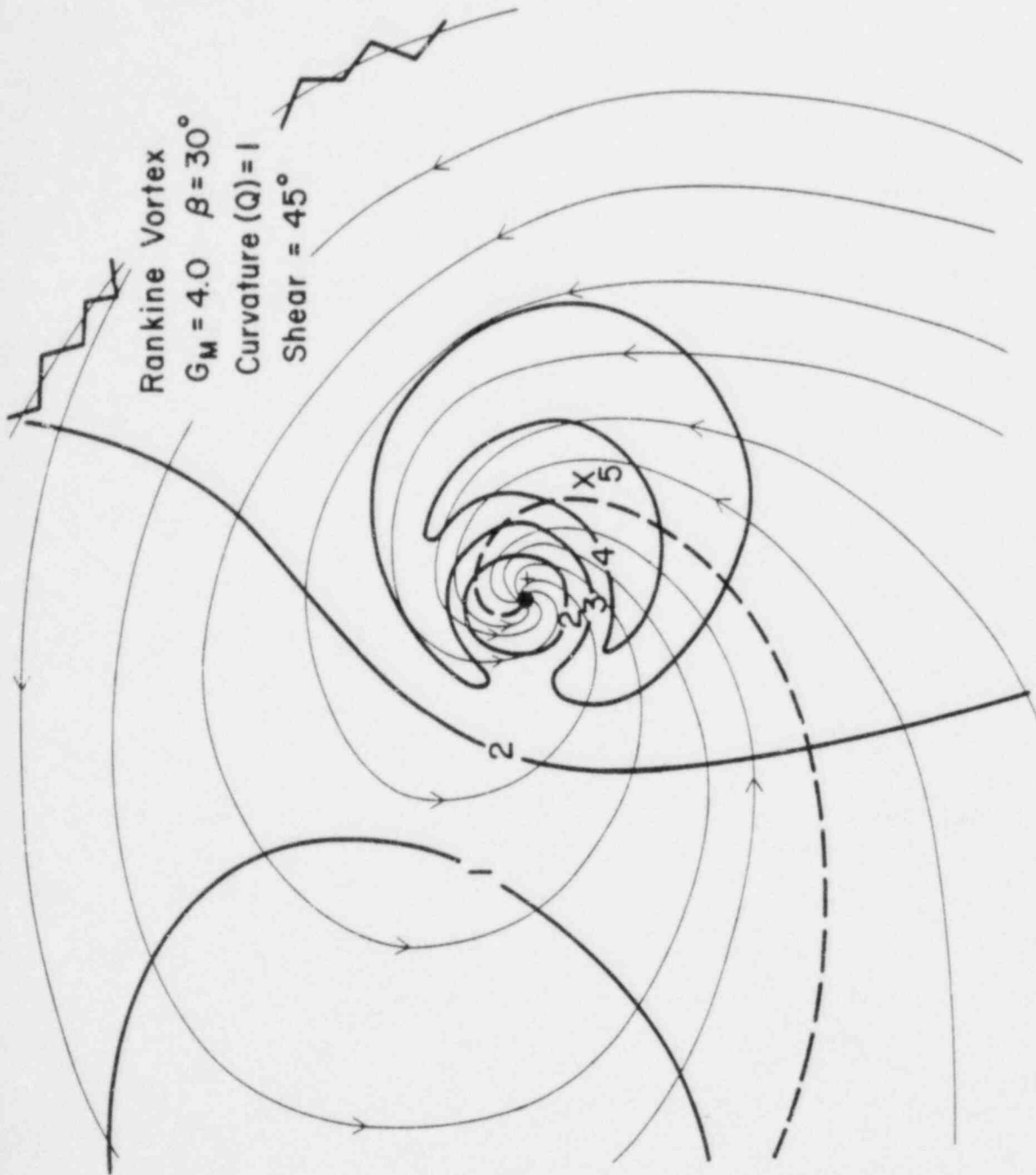


Fig. 18. Isotachs and streamlines for $G_{MAX} = 4$, $\beta = 30^\circ$, shear of 45° , and curvature (Q) = 1.

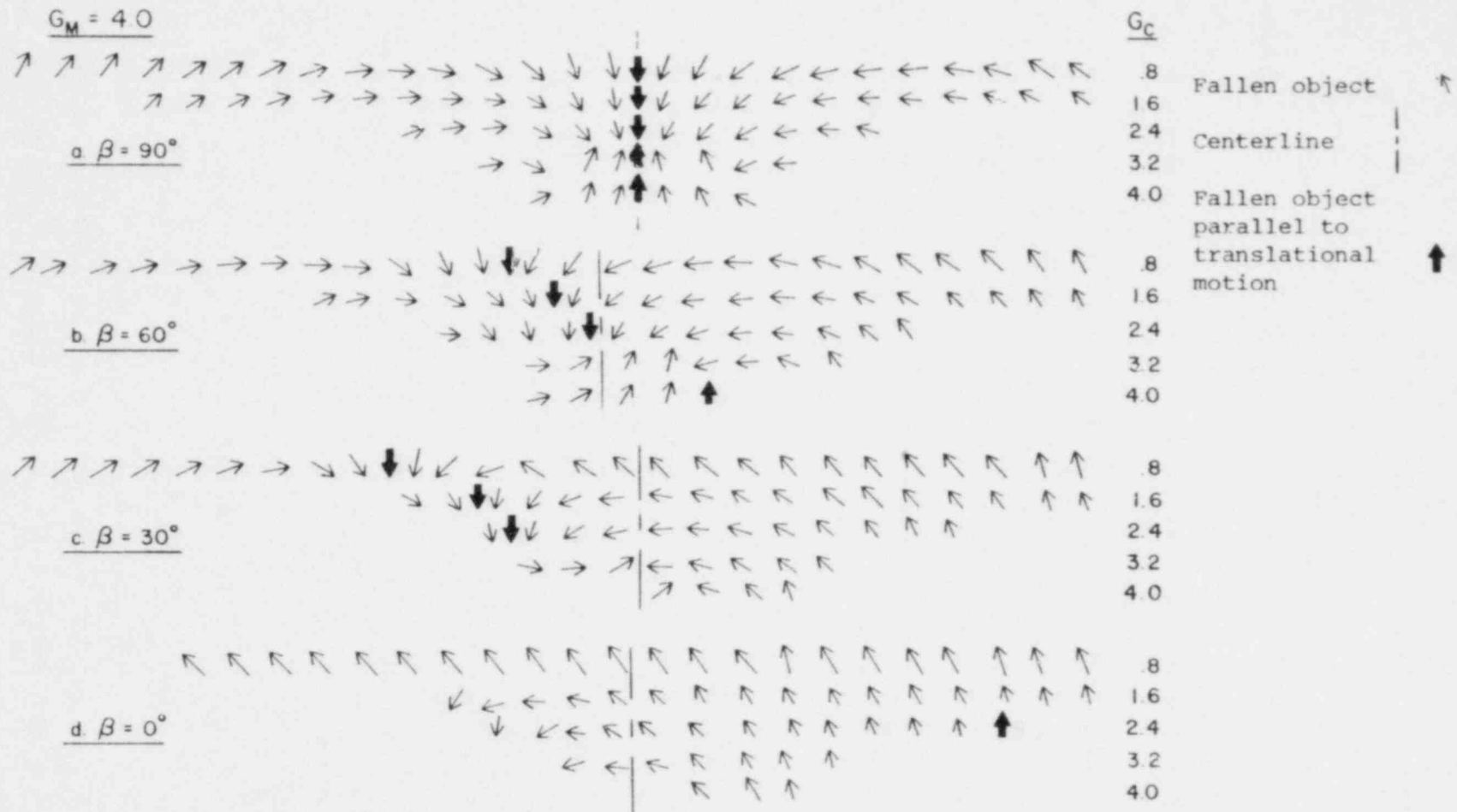


Fig. 19. Swath diagrams for a range of G_{CRIT} and β for $G_{MAX} = 4$.

orientation of the trees on the left side of the tornado track. As G_{CRIT} increases, the wind speeds on the left side of the vortex are not large enough to cause a tree to fall; eventually as the speed necessary for blow-down increases, to say $G_{CRIT} = 4$, damage will only occur to the right of the centerline of the vortex. In a field investigation, this may cause the center of the inferred track to be placed incorrectly. Also, with no inflow in the vortex, the damage may be interpreted as non-tornadic or even as straight line damage.

The effects of radial inflow may be represented by Fig. 19c, for which $\beta = 30^\circ$. With $G_{CRIT} = 0.8$ the trees to either the extreme left or right point nearly in the direction of translation. In the middle, however, a reversal occurs with trees pointing opposite to the direction of translation. It should be noted also that this reversal does not occur at the vortex center but instead to the left of center. Increasing G_{CRIT} to 2.4 causes the reversal to shift further to the right, but still located to the left of the centerline. It will be seen later that as the inflow angle reaches 90° , pure inflow, the reversal is situated along the centerline of the vortex. If $G_{CRIT} = 3.2$, a new pattern occurs; a distinct crossing of the trees becomes apparent. In general, if a reversal is present, trees on either side will point toward (or converging toward) the reversal. However, for trees oriented in the direction of translation both convergence of the trees and divergence of the trees may be present. For the case of pure inflow (Fig. 19a) symmetry is noted. It was stated earlier that the center of the damage swath is also the center of the vortex for $\beta = 90^\circ$.

If $G_{MAX} = 1$, the patterns in Fig. 19 occur, except with no reversal orientation. If $G_{MAX} < 1$, the primary orientation will be in the direction of translation. Therefore, with a weak and/or fast-moving vortex, virtually straight-line winds (with some convergence or divergence) will occur. It should also be noted that the entire swath shifts to the right of the translation line revealing a more circular motion. For uniform outflow, only a pattern of divergence across the swath will be apparent.

Examples of early damage patterns obtained by ground survey are illustrated in Fig. 20. A more realistic presentation of the simulated damage tracks may be obtained by combining many of the same swaths and placing them in a series of rows (as in Figs. 21, 22, 23, 24, and 25). Each of these figures may represent a section out of the whole path or may represent a swath taken at intervals along the path. The figures do not, however, represent the actual path length, unless, of course, the tornado was very short lived.

In Fig. 26 swaths for a Rankine vortex with $G_{MAX} = 4$ and $\beta = 30^\circ$ are shown for a sequence of values of G_{CRIT} . As can be seen, the swaths are not centered at the vortex center. In principle, this would represent a vortex increasing in translational speed and increasing in rotational speed. Such a change in G_{CRIT} could also be due to progressively encountering objects less able to withstand the vortex winds, where the translational and rotational properties remain constant.

For an evolving vortex, the inflow angle β may change with time. Fig. 27 displays three different examples of damage patterns that would result for a vortex with $G_{MAX} = 4$, inflow angles increasing from 0° to 90° , and $G_{CRIT} = 0.8, 1.6, \text{ and } 2.4$. Physically this could represent a vortex beginning with purely cyclonic rotation with no inflow, with inflow later increasing to $\beta = 90^\circ$ (pure inflow). An interesting feature arises in each of these three cases. This feature is represented by the shifting of the damage patterns characteristic to the right. It should also be noted that even though the characteristic pattern shifts to the right the swaths seem to represent the vortex moving in a non-rectilinear fashion to the left even though the vortex center has not changed position.

Another type of evolution is simulated if G_{MAX} changes during the lifetime of the vortex. This would imply that the rotational intensity and/or the speed of translation varies. For example in Fig. 28, G_{MAX} is increasing from 1.0 to 10.0. This would represent an intensification of the vortex with time. As in the cases represented in

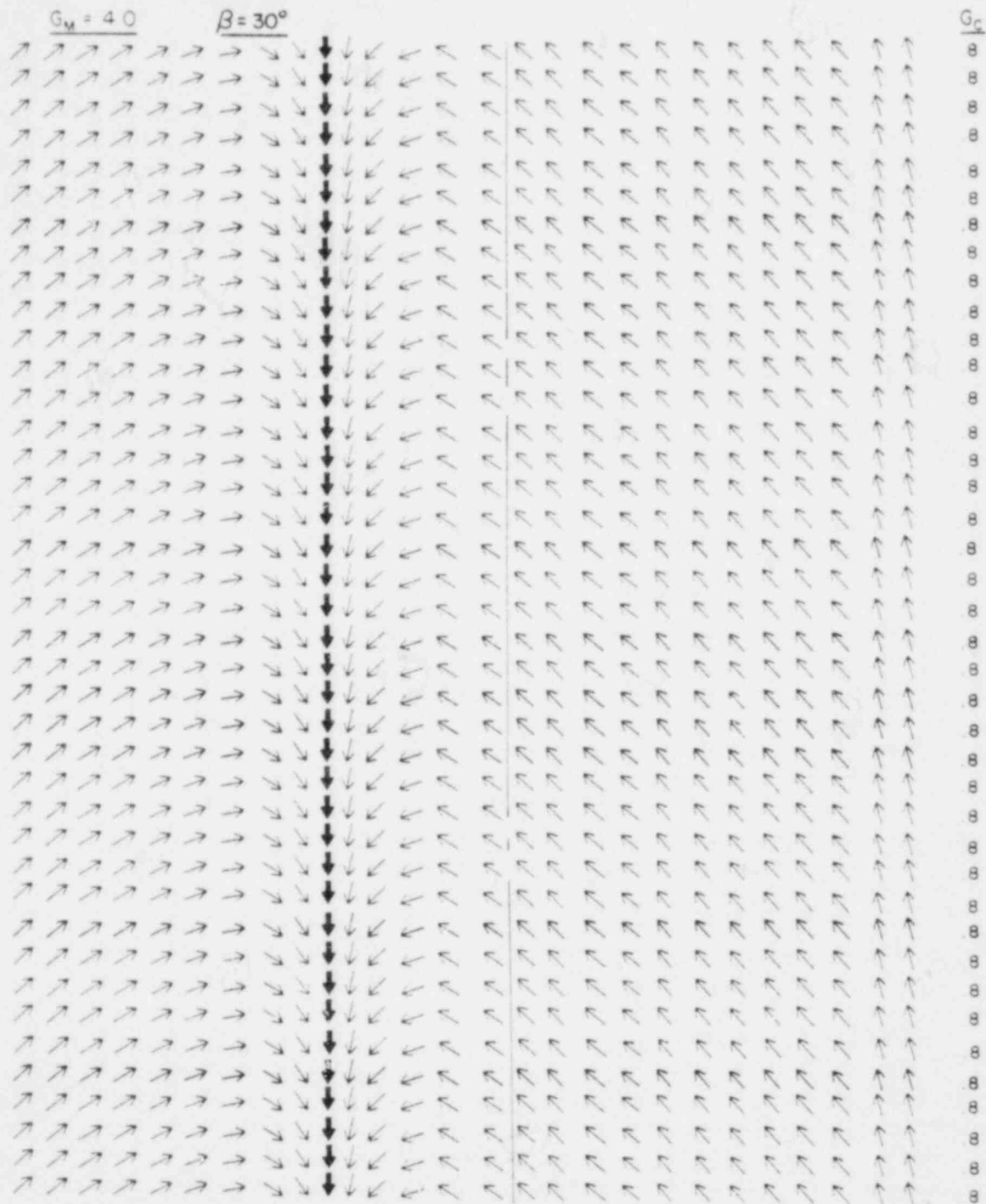


Fig. 21. Damage swath for $G_{MAX} = 4$, $\beta = 30^\circ$, and $G_{CRIT} = 0.8$.

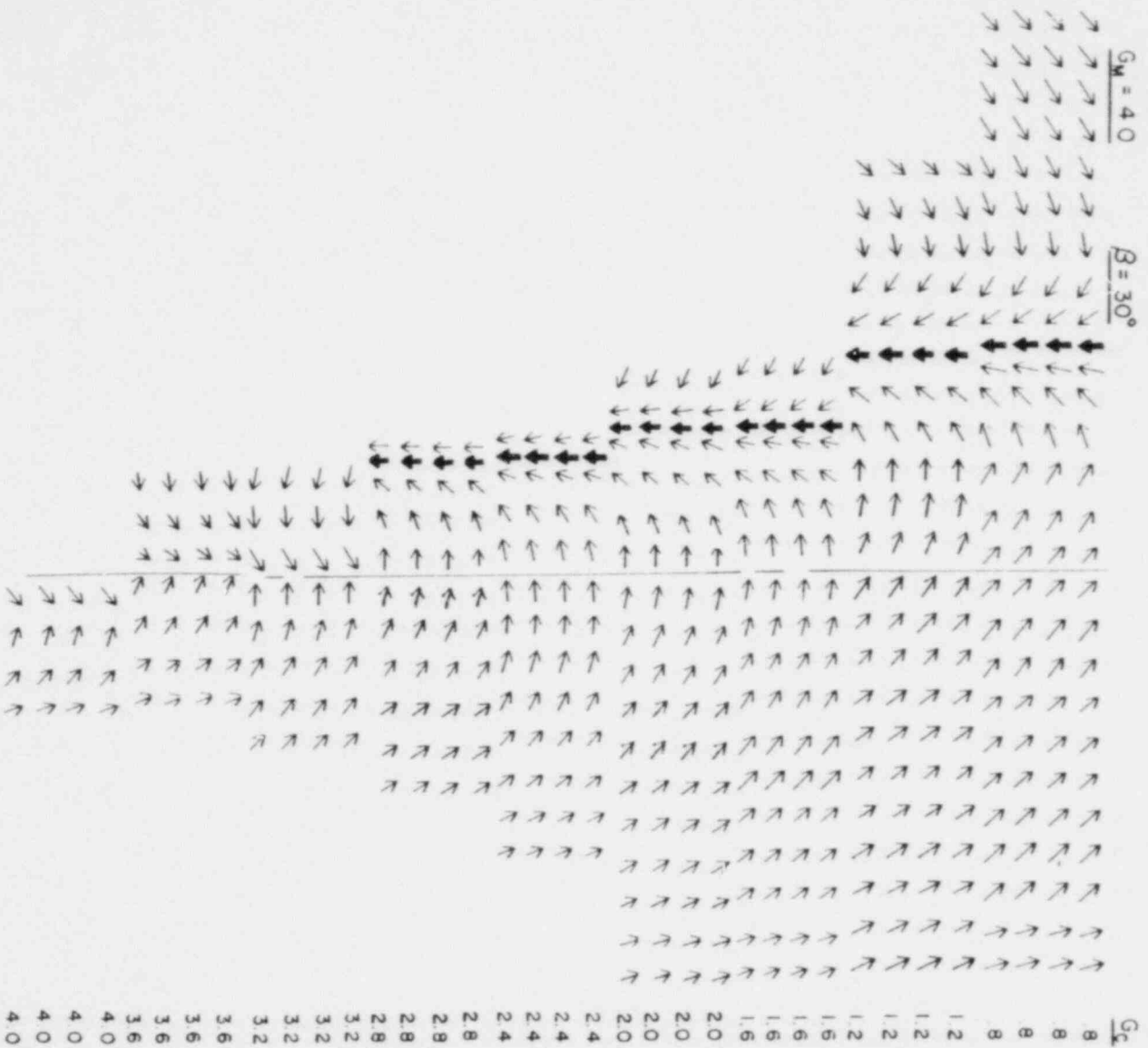


Fig. 26. Damage swath for $G_{MAX} = 4$ and $\beta = 30^\circ$ for a sequence of different γ_{CRIT} .

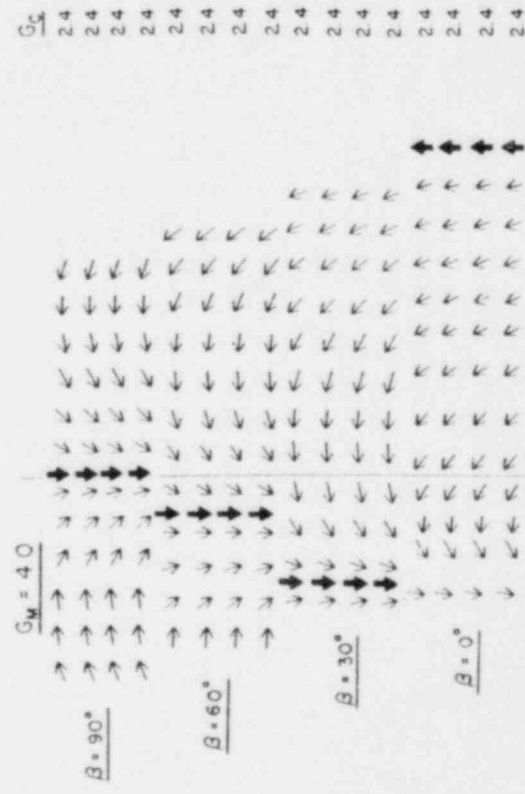
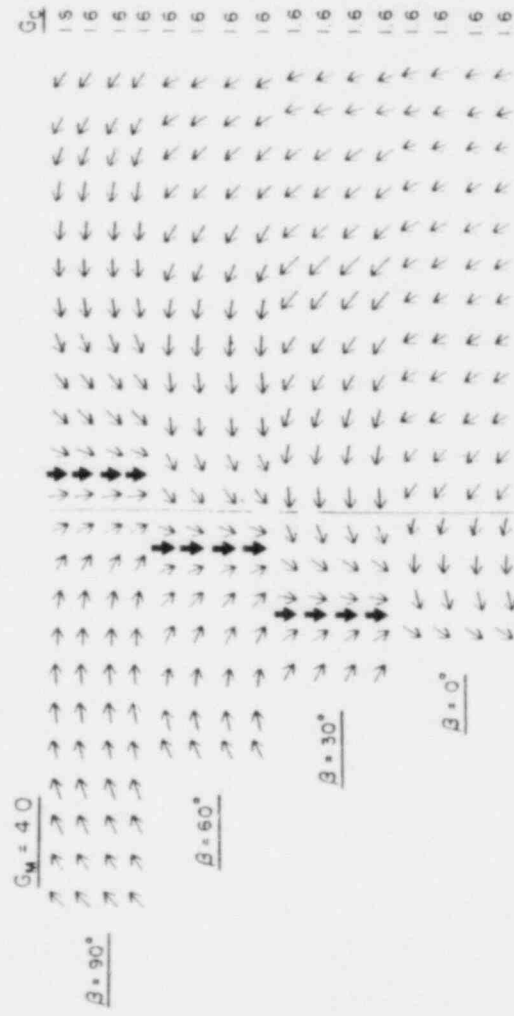
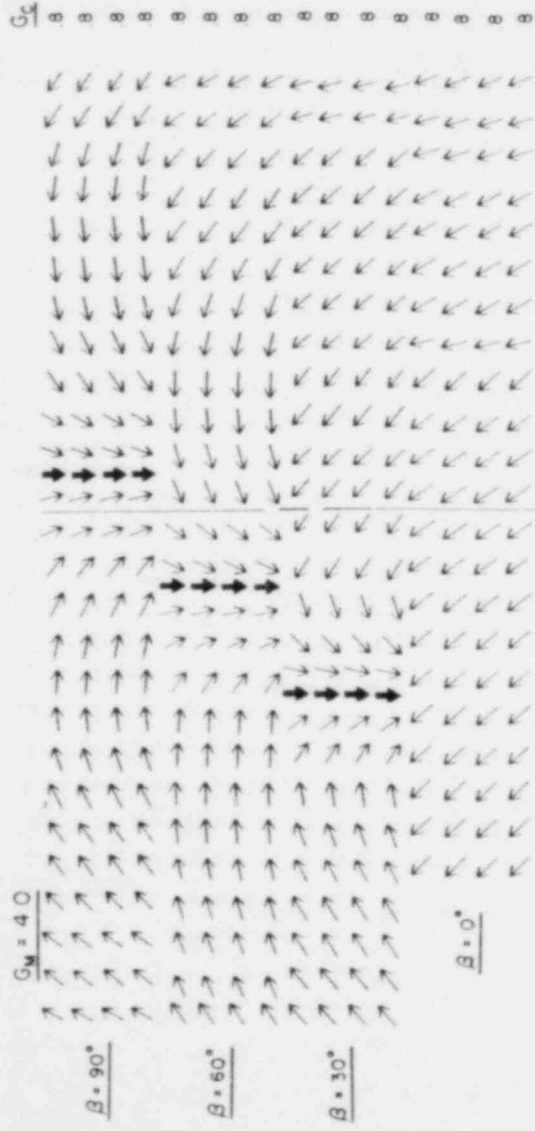


Fig. 27. Damage swaths for $G_{MAX} = 4$, β increasing from 0° to 90° and for $G_{CRIT} = 0.8, 1.6, \text{ and } 2.4$.

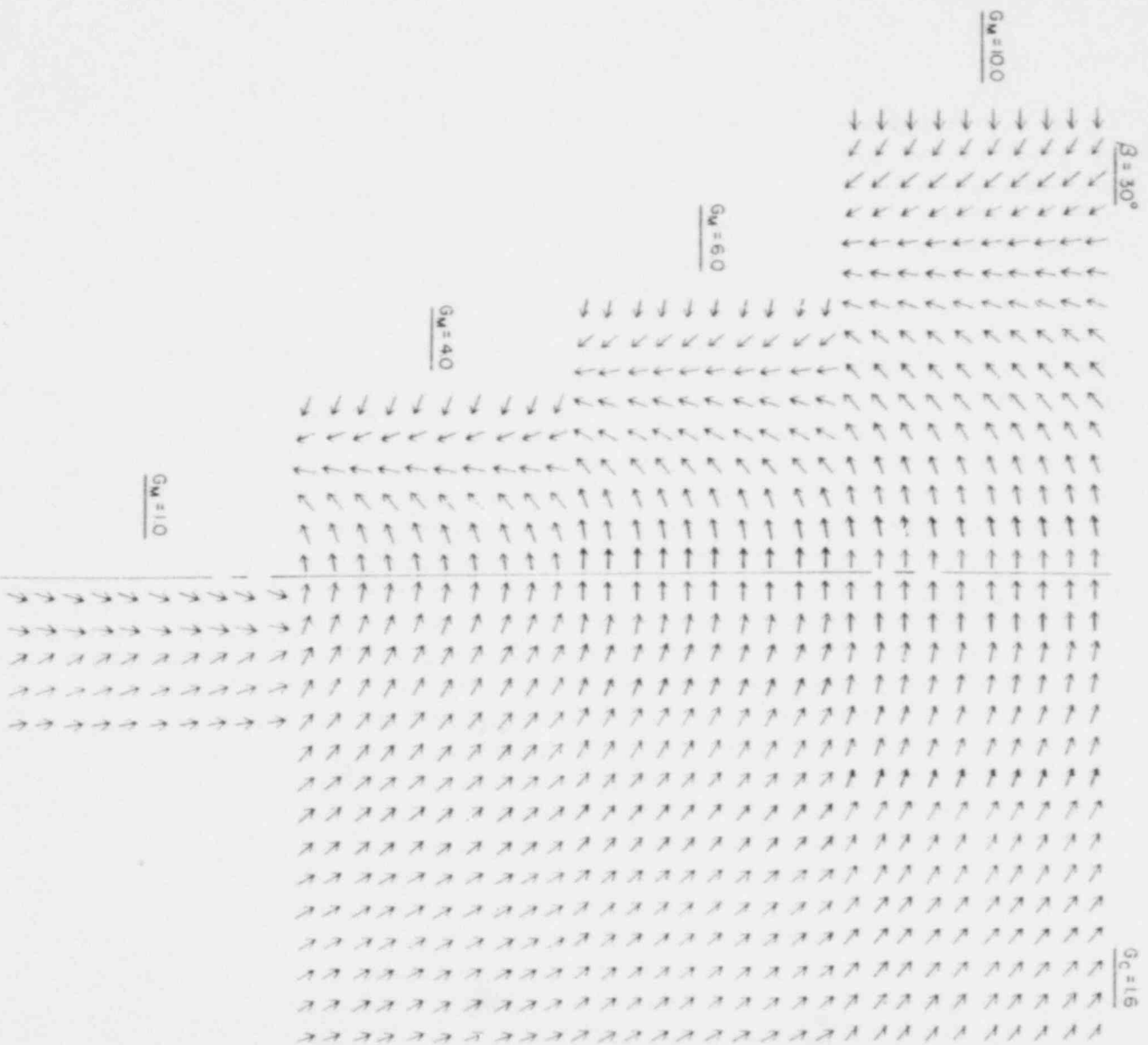


Fig. 28. Damage swath with G_{MAX} increasing from 1.0 to 10.0, $\beta = 30^\circ$, and $G_{CRIT} = 1.6$.

Fig. 27 and Fig. 28, misinterpretations could be made in terms of the actual vortex center and the direction of translation.

A more realistic case of an evolving vortex damage pattern is shown in Fig. 29, with both G_{MAX} and β changing. In the beginning of the evolution process, where $G_{MAX} = 1$ and $\beta = 90^\circ$, the vortex is very weak and there exists pure inflow. The damage pattern is extremely narrow and is centered along the vortex center line. As G_{MAX} increases to 4, the vortex becomes stronger in rotational speed, while the translational velocity remains constant. The inflow angle decreasing to 60° allows more circular motion to exist. The damage pattern increases in width with the largest width increase on the right side where the maximum winds occur. The damage pattern is not symmetric to the center line of the vortex translation motion. Further evolution is shown where G_{MAX} changes to 6 and β to 30° . The damage pattern continues to increase in width as the vortex becomes stronger and as the inflow angle decreases. The final stage in the evolution is represented by a change in vortex structure. The vortex becomes extremely intense, with G_{MAX} increasing to 10, as the inflow angle becomes variable. The vortex becomes two-cell in structure with outflow occurring inside the radius of maximum wind and inflow outside this radius. It is important to note that the point of reversal changes position with respect to the vortex center line. The vortex is simulated to be traveling in a rectilinear fashion and should be kept in mind when trying to fit observed damage patterns to this simulated case.

Even more complicated swaths are generated if the critical speed for failure across the width of the tornado is non-uniform. For example in Fig. 30, the critical speed G_{CRIT} increases from a value of 0.5 on the far left to 4.0 on the far right. Actual damage of this kind might be interpreted as two tornadoes with an area of no damage between them. In Fig. 31, G_{CRIT} decreases from 4.0 on the left to 0.5 on the right side. Trees are not effected on the extreme left side of the vortex because of the weak vortex velocities and the large G_{CRIT} values. As

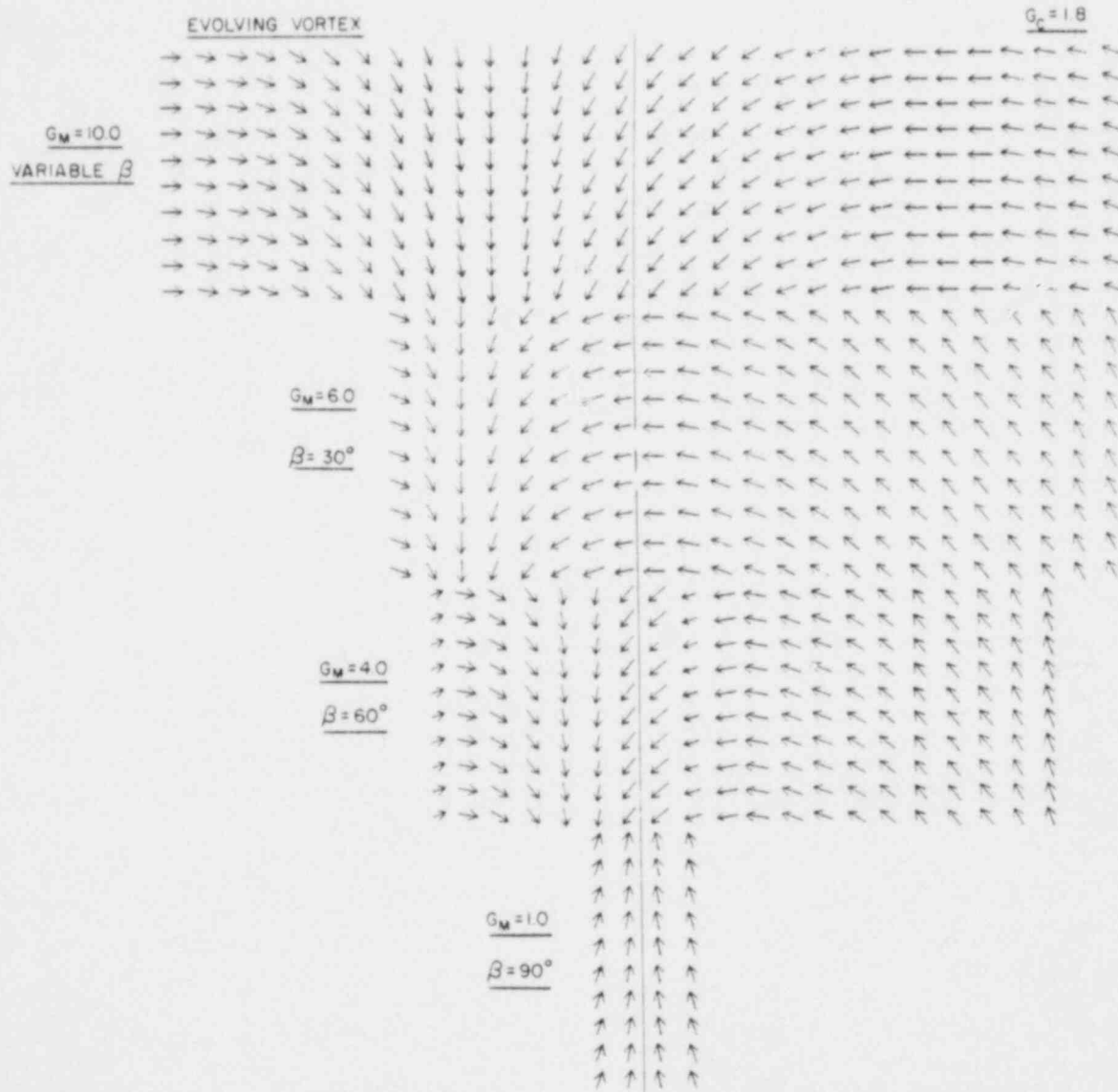


Fig. 29. Damage swath for an evolving vortex for $G_{CRIT} = 1.8$ with varying G_{MAX} and β .

$G_M = 4$
 $\beta = 30^\circ$

G_C VARIABLE

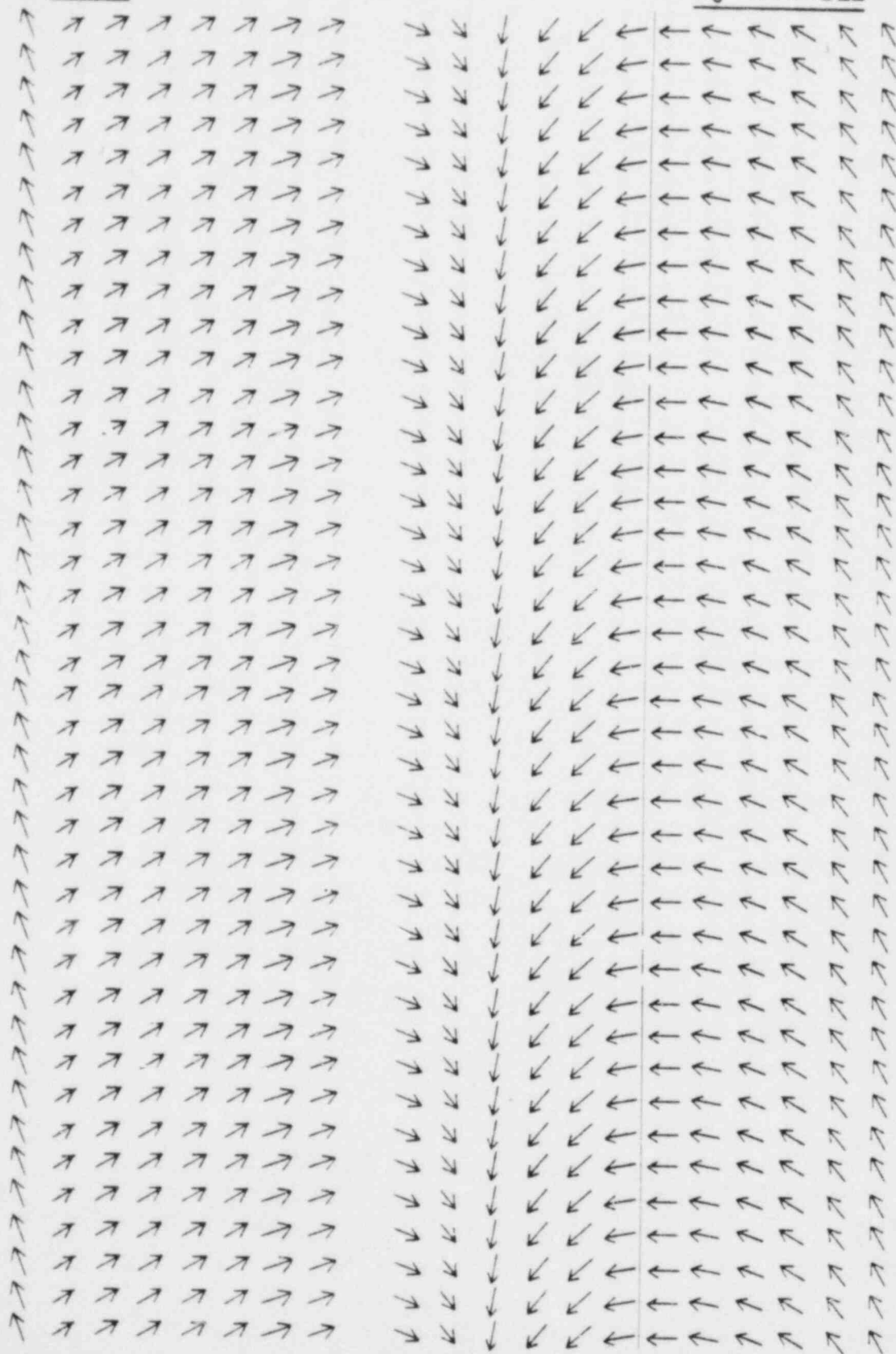


Fig. 30. Damage swath for $G_{MAX} = 4$, $\beta = 30^\circ$, and G_{CRIT} increasing left to right from 0.5 to 4.0.

$$\frac{G_M = 4}{\beta = 30^\circ}$$

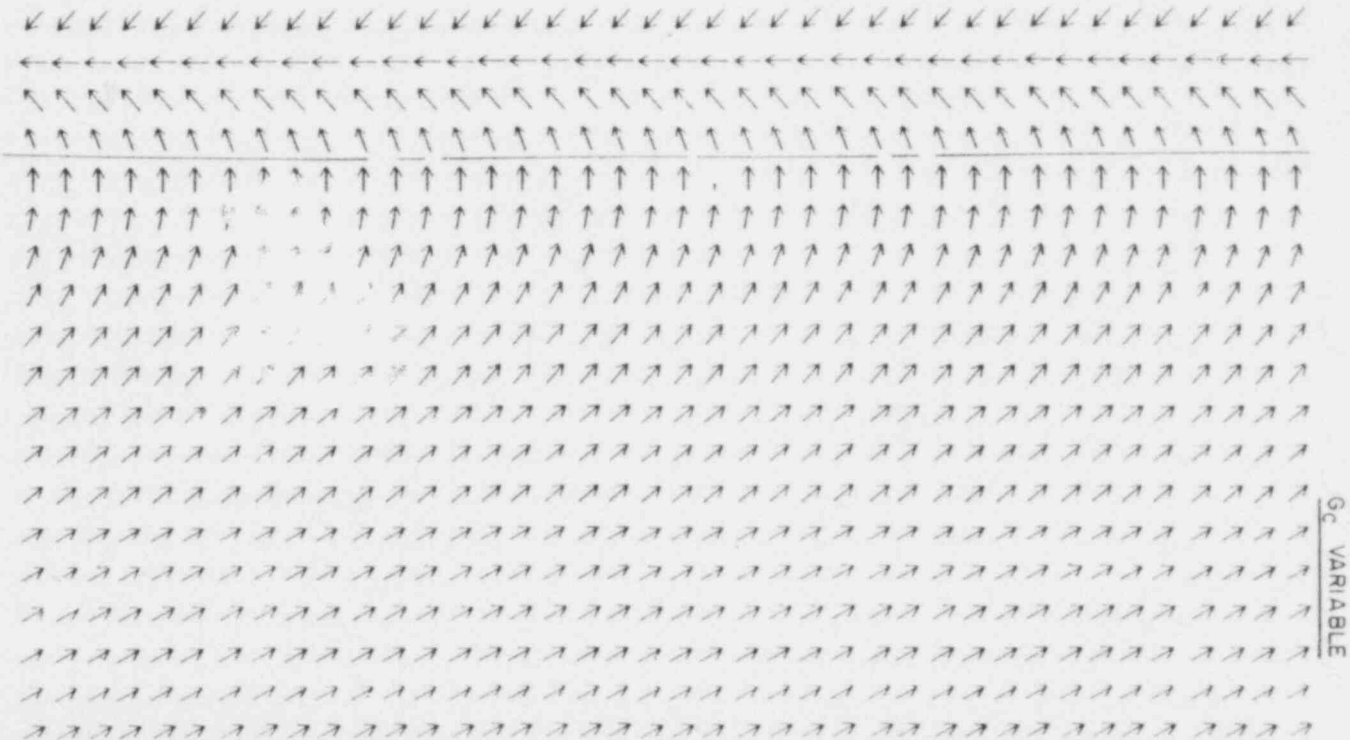


Fig. 31. Damage swath for $G_{MAX} = 4$, $\beta = 30^\circ$, and G_{CRIT} decreasing left to right from 4.0 to 0.5.

in previous cases the center of the vortex is not necessarily where the reversal occurs and should be noted by the investigator of tornado damage tracks. In Fig. 32, G_{CRIT} increases linearly from 0.5 on the sides to 4.0 along the centerline of the vortex. This simulated swath has a large separation area with no tree failure. The type of damage could also be confused with two tornadoes acting together. These cases for the variable G_{CRIT} could help investigators realize that there was actually one tornado rather than two.

Using the vortex translated by rectilinear flow Letzmann (1924) categorized fundamental patterns of damage into five basic patterns for combinations of G_{MAX} , β , and G_{CRIT} :

1. convergence
2. divergence
3. orientation in the translation direction with some convergence to either side,
4. orientation counter to the translation along the middle of the swath, and
5. convergence with a marked crossing near the swath centerline.

These are schematically depicted in Fig. 33. The inflow angles are in terms of the angle α where $\beta = \alpha + 90^\circ$; $G_{MAX} < 1$ characterizes Type I; with increasingly large G_{MAX} , Types II-IV arise.

Special Cases

The non-dimensional vortex model was developed in part so that wind fields and damage patterns could be obtained for arbitrary vortex models. These need only have specified distributions of rotational velocity and inflow angle with respect to the radius along with specified critical windspeeds.

One model of interest is the U.S. Nuclear Regulatory Commission Design Basis Tornado. The NRC vortex is specified to have a Rankine vortex velocity distribution, an inflow angle of $26^\circ 34'$ and a maximum rotational component of 130 m/s (290 mph). Placing these parameters into the model with $G_{MAX} = 4.0$ yields $V_{TRAN} = 32.5$ m/s (which is a

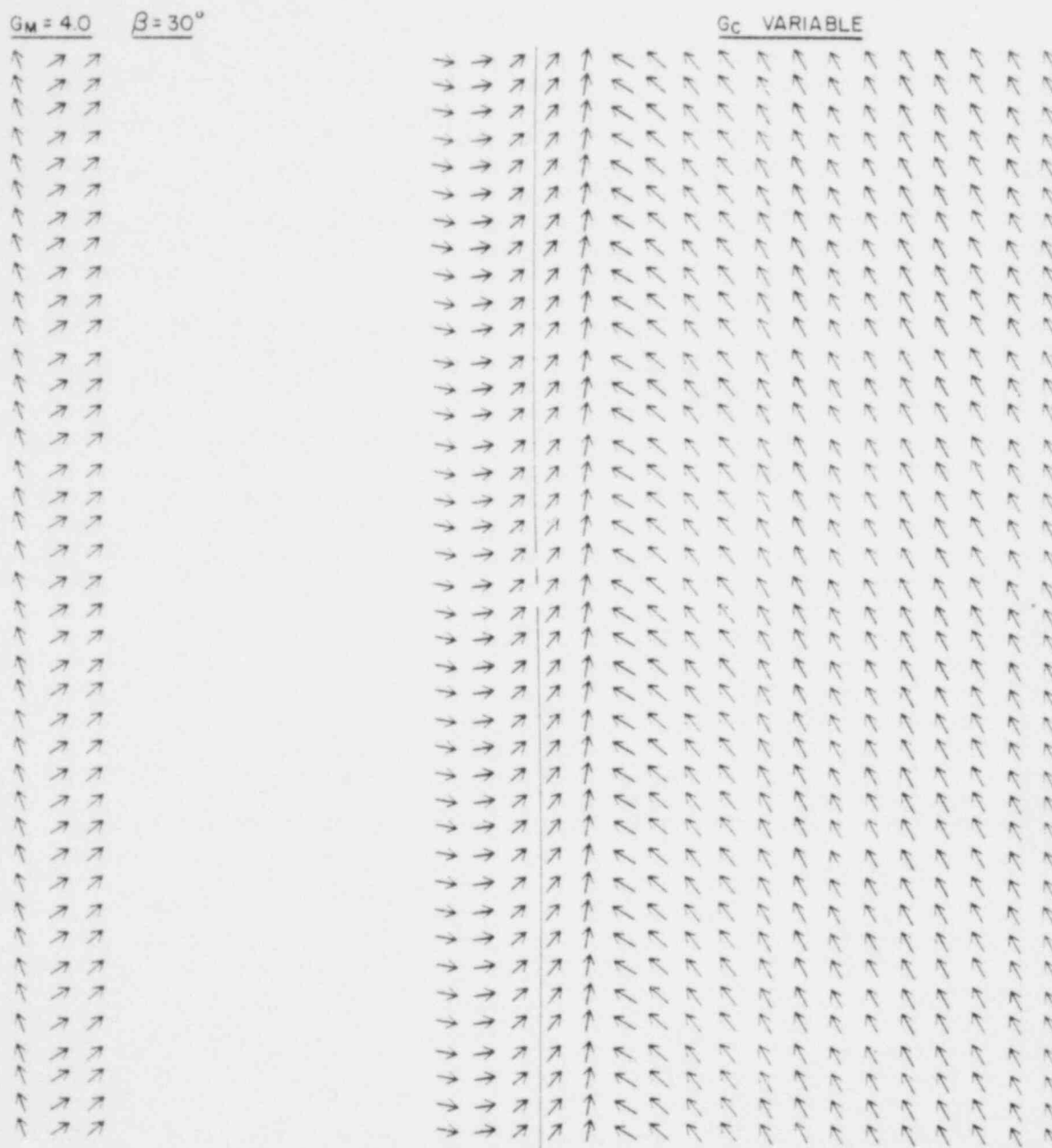


Fig. 32. Damage swath for $G_{MAX} = 4$, $\beta = 30^\circ$, and G_{CRIT} increasing from 0.5 on the sides to 4.0 along the centerline.

	Form a $\alpha = 0^\circ$	Form b $\alpha = \sim -30^\circ$	Form c $\alpha = \sim -60^\circ$	Form d $\alpha = -90^\circ$	
TYPE I					Swath types
					Form e $\alpha = \sim -135^\circ$
TYPE II					
					Form f $\alpha = 180^\circ$
TYPE III					
TYPE IV					

Fig. 33. Characteristic swath types (after Letzmann, 1924).

rather fast moving vortex). The characteristics of the wind field and swath patterns are depicted in Fig. 34. Also, the translational speed of 32.5 m/s is used to generate the swaths corresponding to $V_{CRIT} = 25, 35, 45, 55, 65, 75, 85, \text{ and } 95 \text{ m/s}$. In Fig. 34 the isotach pattern and streamlines are very similar to Fig. 3 except that in Fig. 3 $\beta = 30^\circ$ and dimensional values are assigned to the isotachs. The analysis reveals no unexpected patterns of wind or damage.

Another tornado model investigated is the one formulated by Fujita, 1977b. The formulation adopts the Rankine vortex profile for the tangential wind field. The radial component of the rotational motion varies with the radius as does β . As before, the radius at which the maximum wind speed occurs is $r = 1$. Inside $r = 1$, two cores are defined. In the inner core, there is no radial component, implying only circular motion. The outer core has a variable inflow angle that obeys $\alpha = \arctan(a \tan \alpha_0)$ where a depends on n and r .

$$a = \frac{r^2 - n^2}{r^2 (1 - n^2)}$$

Also n depends on r (at $r = 150 \text{ m}$, $n = 0.509$). In this model, the maximum rotational component is set at 130 m/s with $\alpha_0 = -36.87^\circ$. Fig. 35 provides the wind field and damage patterns for these parameters specified in the model. For $G_{MAX} = 4.0$, then $V_{TRAN} = 32.5 \text{ m/sec}$. The only marked difference in this wind field and that of Fig. 3 occurs near the core of the vortex. In Fujita's model the inner core of pure circular motion causes this difference. The damage patterns are very similar to the ones found in Fig. 19c.

The final special case is four subvortices embedded in a larger parent vortex (Fig. 36), where the parent vortex system consists only of solid rotation. The design of the problem includes the vector addition of the rotational velocity of the subvortex, the translational shear and curvature, and the translation of the entire parent vortex system. The analysis of the streamlines reveals five distinct patterns. The first pattern of interest is that of the subvortex located directly

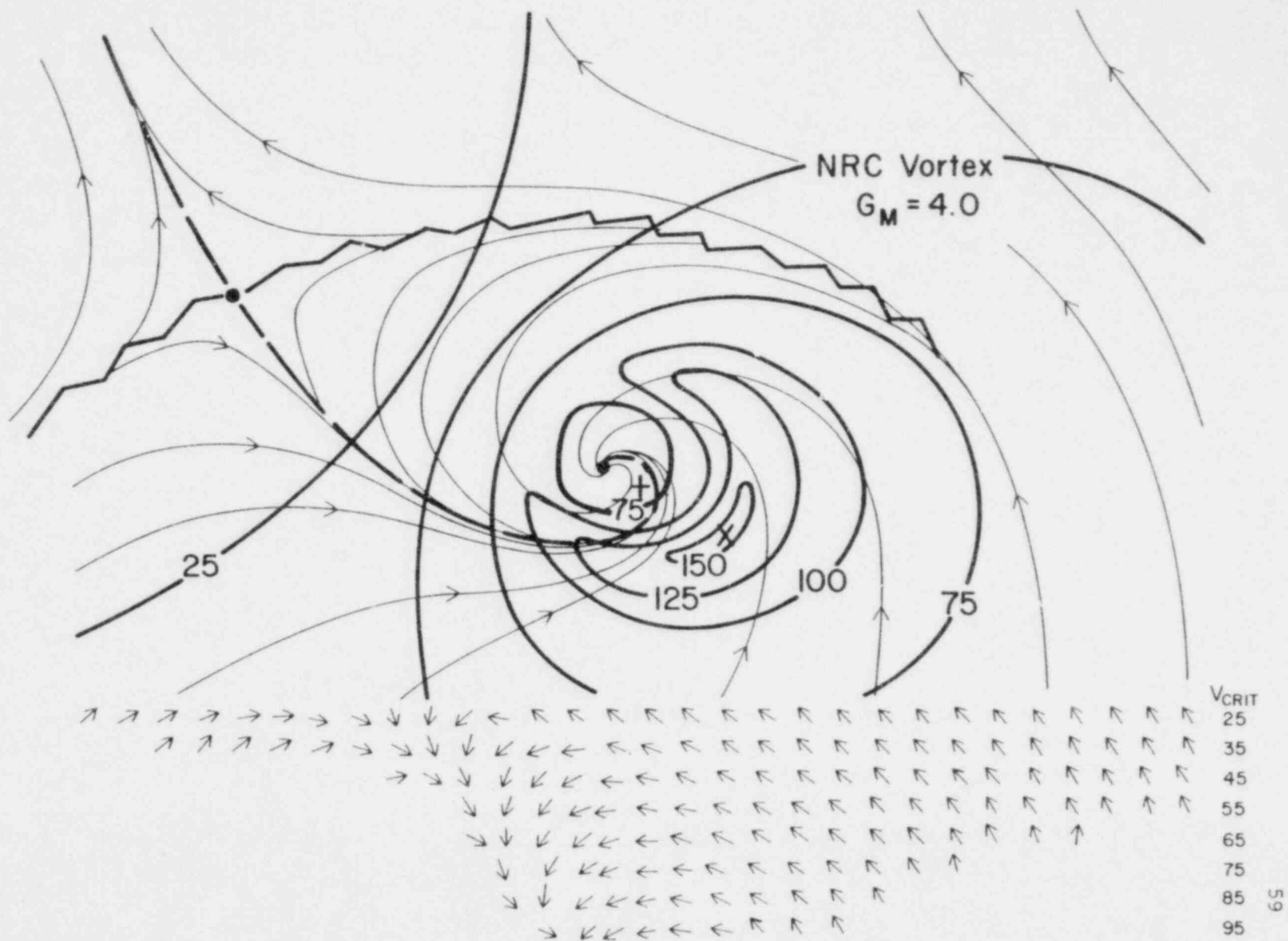


Fig. 34. Isotachs, streamlines, and damage swaths for the NRC vortex.

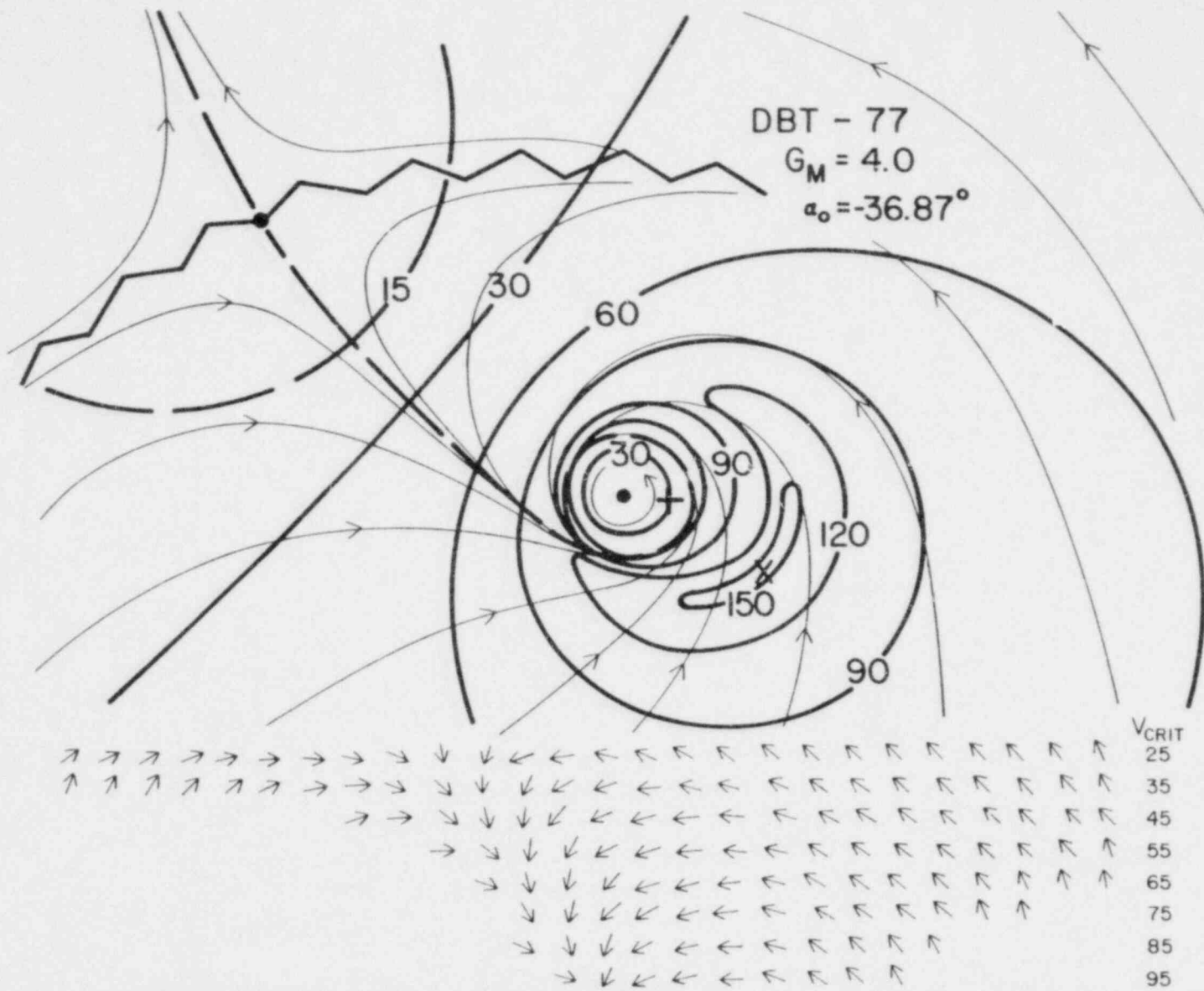


Fig. 35. Isotachs, streamlines, and damage swaths for Fujita's DBT-77.

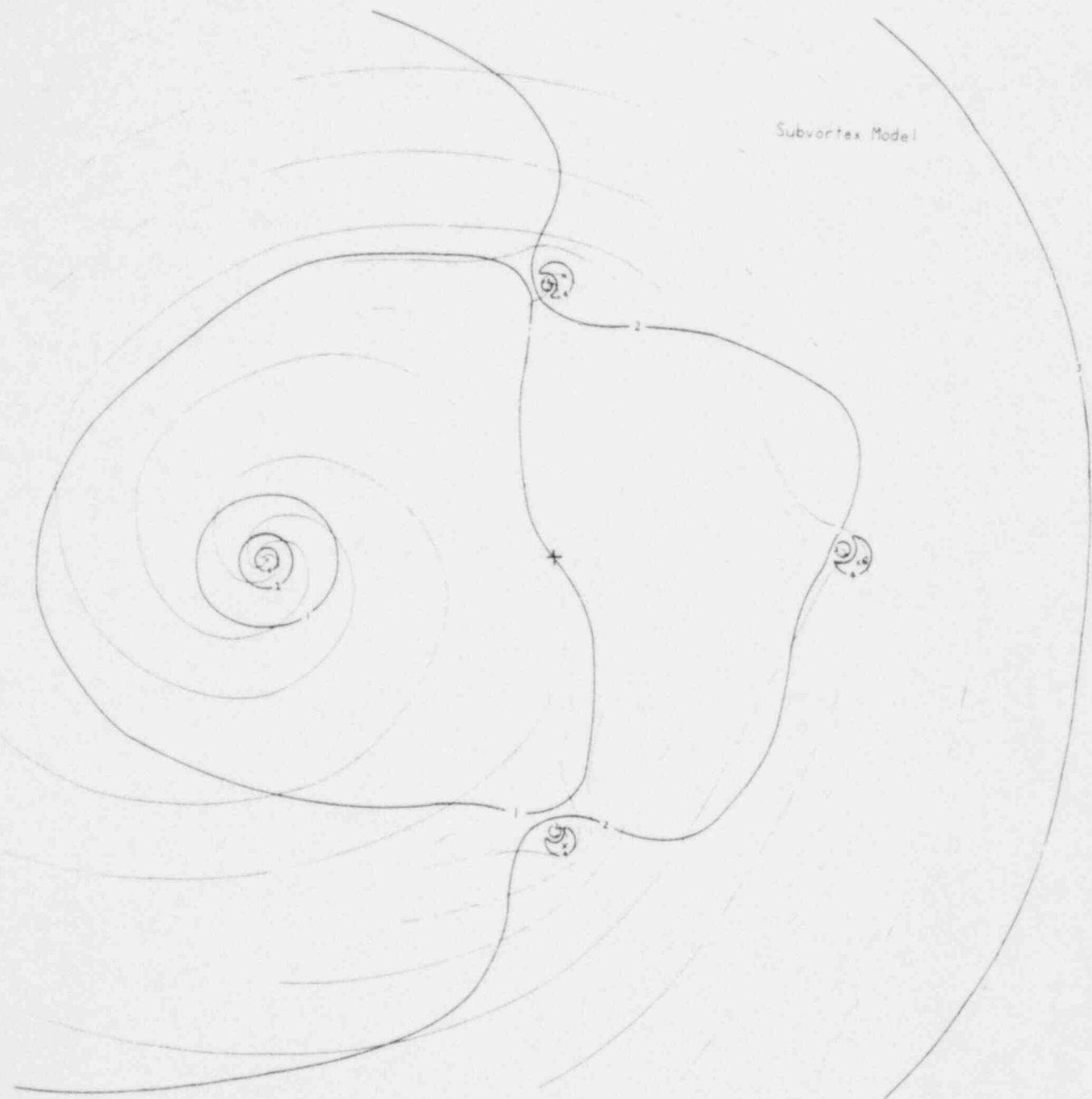


Fig. 36. Isotachs and streamlines for the subvortices model.

to the left of the parent vortex center. The streamlines located around this subvortex center are very much like the streamlines associated with a non-translating vortex with a small inflow angle. The second subvortex of interest is the one located directly below the parent vortex center. Its streamline pattern resembles that of a translating vortex with $\beta \approx 70^\circ$. The subvortex, directly to the right of the parent vortex center, has streamlines very similar to those where $\beta = 30^\circ$ and $G_{MAX} > 1$. The last subvortex in the model, placed directly above the parent vortex center has an apparent inflow angle of approximately -10° . The fifth streamline pattern of interest is the combined effect of the four subvortices and the parent vortex. Except for the streamlines in the close proximity of the subvortices, the pattern closely resembles that of a solid rotational vortex in translation.

In analyzing the isotachs it is found that the weakest maximum speeds around an individual subvortex occur in the subvortex located directly to the left of the parent vortex center. The strongest speeds occur in the subvortex directly to the right of the center. The subvortices located above and below the parent vortex center are similar in magnitude to the maximum winds located in the right rear and right forward quadrants, respectively for the subvortices.

CHAPTER VI

CONCLUSION

The principle objective of this study, to better understand near-ground tornado wind fields and damage patterns, has been approached by means of numerical simulations involving a simplified model. The results obtained should aid engineers in designing structures to withstand the "average" tornado and should assist scientists interpreting tornado structure from damage patterns.

This study has been based primarily on Letzmann's work in the early Twentieth Century. His investigations of tornadoes were far ahead of their time. In this study the basic vortex model used has been the Rankine vortex. Translational motion was added vectorially to the model to obtain the simulated wind fields and hence the damage patterns in and around the vortex. It has been noted that the basic wind field pattern depended on two parameters: G_{MAX} , the ratio of the maximum rotational wind to the speed of translation and β , in inflow angle. The damage pattern depends on an additional parameter G_{CRIT} , the ratio of the critical speed for failure to the translational speed. Using these parameters it has been possible to obtain key features in the patterns derived from the non-dimensional formulation.

For G_{MAX} values greater than one (signifying the stronger tornadoes) there exist two areas of calm and one area of maximum wind. One area of calm will be located within the radius of maximum wind and the other beyond this radius. Most isotachs will be nearly circular, except for the range of $G_{MAX} \pm 1$ for which the isotachs are crescent-shaped. The area of maximum wind will be located to the right of the vortex center usually in the rear quadrant depending on the angle of inflow, β . The areas of calm will be located in the left forward quadrant also depending on the inflow angle. For $\beta = 0^\circ$ (Fig. 5), the maximum wind will be located directly to the right of the vortex center

and the areas of minimum directly to the left of the center. As the inflow angle increases from $\beta = 0^\circ$ (Fig. 3), the whole pattern rotates clockwise to the new value of inflow angle. The new position for the calm points and the maximum point will be located in the left forward and right rear quadrants, respectively. For a two-cell vortex the internal calm point will shift to the rear and the external calm will remain as in the one-cell case. As G_{MAX} becomes larger and larger (Fig. 4) the position of maximum wind remains the same, the internal calm approaches the vortex center, and the external calm moves further away from the center.

For the case of large translational shear (Fig. 13) the external calm point is shifted further away than in the no-shear case. Also the isotach pattern is altered somewhat. As the shear decreases (Fig. 14) the pattern begins to resemble that of straight translational flow (Fig. 3).

A similar situation occurs for the addition of curvature into the translational flow. For a large radius of curvature (Fig. 16) the flow field resembles that of no curvature (Fig. 3). As the curvature becomes smaller (Fig. 15) the external calm moves toward the horizontal center line that extends through the vortex center.

For the translational shear and curvature case (which probably more closely resembles what actually happens in nature) illustrated in Fig. 17, the basic patterns resemble Fig. 3 (no translational shear or curvature case). With the addition of large shear and small radius of curvature (Fig. 18) the wind field is similar to that of a stationary solid rotational vortex.

Two other important features that appear in the wind field are the convergence and divergence lines. These meet at the external calm point. The most important line appears to be that which wraps into the vortex center through an area of strong winds because of the similarities to the dust band (Golden and Purcell, 1975a).

Researchers have long been interested in the total wind fields of vortices such as those formulated here. Similar wind fields have been recorded for dust devils (Peterson, 1976), tornadoes (Golden and

Purcell, 1975a), waterspouts (Golden, 1974), mesocyclones (Brandes, 1977) and hurricanes (Shea and Gray, 1973).

Characteristics of swath patterns have been formed for several combinations of G_{MAX} and β and for a range of G_{CRIT} . In general, four swath types occur (Fig. 33) depending on β . For $G_{MAX} < 1$, Type I patterns occur. For $G_{MAX} > 1$, Types II-IV occur. Form "a" corresponds to a no inflow while "b", "c", and "d" correspond to an increasing inflow. Forms "e" and "f" refer to outflow patterns.

Examples of a hypothetical section of the damage track have been illustrated for various cases. Figs. 26, 27, 28, and 29 may represent damage as a type of evolution takes place in and around the vortex. Cases in which objects of non-uniform resistance were arrayed across the width of the damage track were also presented. From these it has been noted that areas of no damage could occur in the swath pattern due to the non-uniformity in the strength of objects.

Two special cases have been obtained to compare the patterns of streamlines, isotachs, and swaths. No significant differences were seen between these patterns. Also, a special case has been obtained for the idea of subvortices embedded in a larger vortex. This simplified case has revealed a combination of effects which already had existed earlier in patterns of single vortices, yet the general pattern is of special interest also. The pattern in general has been represented as a solid rotational vortex in translation. The only disturbance in the patterns have been near the location of the subvortices. It has been noted that the subvortices and the larger parent vortex could exist together and yet remain to show their independent patterns of flow.

LIST OF REFERENCES

- Anonymous, 1950: A dissertation on the whirlwind which damaged a great part of Rome, on the night of the 11th of June, 1749, by Father Boscovich. The Monthly Review, December, 148-154.
- Brandes, E., 1977: Gust front evolution and tornado genesis as viewed by Doppler radar. J. Appl. Meteor., 16, 333-338.
- Brooks, E. M., 1951: Tornadoes and related phenomena. Compendium of Meteorology, 673-680.
- Fujita, T., 1977a: Anticyclonic tornadoes. Weatherwise, 30, 51-64.
- Fujita, T., Abbey, R.F., Jr., Workbook of tornadoes and high winds. Report for U.S. Nuclear Regulatory Commission, University of Chicago, to be published June 1982 as NUREG/CR-1447.
- Golden, J., 1974: The life cycle of Florida Keys Waterspouts, I, II. J. Appl. Meteor., 13, 676-709.
- _____, and D. Purcell, 1975a: Photogrammetric analyses for the Great Bend, Kansas, tornado of 30 August 1974: acceleration and asymmetries. Mon. Wea. Rev., 87, 207-216.
- Kincer, J., 1937: Reply to Koschmieder. IMO, Klimat. Komm., Publ. no. 38, 88-90.
- Letzmann, J., 1918: Tromben in Ostbaltischen Gebiet. Sitz. Ber. Naturforsch. Gesel. Univ. Dorpat, 24, 7-46.
- _____, 1924: Das Bewegungsfeld im Fuss einer fortschreitenden Wind-oder Wasserhose. Acta Comm. Univ. Dorpat, A6, 1-136.
- _____, 1928: Zur Methodik der Trombenforschung. Meteor. Zeit., 45, 434-439.
- _____, 1937: Richtlinien zur Erforschung von Tromben, Tornados, Wasserhosen and Kleintromben. IMO, Klimat. Komm., Salzburg, Publ. no. 38, 91-110.
- Ludlam, D., 1970: Early American Tornadoes 1586-1870, American Meteorological Society, Boston, 219 p.
- Mal'bakhov, V. M., 1972: Investigation of the structure of tornadoes. Izv. Atmos. Ocean. Phys., 8, 8-14
- Martins, C. L., 1850: Anweisung zur Beobachtung der Windhosen oder Tromben. Ann. der Physik (Poggendorfs), 81, 444-467.
- Peterson, R. E., 1976: In pursuit of dust devils. Weatherwise, 29, 184-189.
- _____, April 1981: Kinematics of translating tornado wind fields. Report for U.S. Nuclear Regulatory Commission, Texas Tech University, NUREG/CR-2014.

- Sandstrom, J. W., 1909: Über die Bewegung der Flüssigkeiten. Ann. Hydro. Maritim. Meteor., 37, 242-254.
- Shea, D. J., and W. M. Gray, 1973: The hurricanes inner core region I. Symmetric and asymmetric structure. J. Atmos. Sci., 30, 1544-1564.
- Wegener, A., 1917: Wind-und Wasserhosen in Europa, Braunschweig, 301 p.

NRC FORM 335 (7-77)		U.S. NUCLEAR REGULATORY COMMISSION BIBLIOGRAPHIC DATA SHEET		1. REPORT NUMBER (Assigned by DDC) NUREG/CR-2557	
4. TITLE AND SUBTITLE (Add Volume No., if appropriate) Simulated Tornado Wind Fields and Damage Patterns				2. (Leave blank)	
7. AUTHOR(S) Dean R. Metcalf and Richard E. Peterson				3. RECIPIENT'S ACCESSION NO.	
9. PERFORMING ORGANIZATION NAME AND MAILING ADDRESS (Include Zip Code) Atmospheric Science Group Texas Tech University P.O. Box 4320 Lubbock, Texas 79409				5. DATE REPORT COMPLETED MONTH August YEAR 1978	
12. SPONSORING ORGANIZATION NAME AND MAILING ADDRESS (Include Zip Code) Division of Health, Siting, and Waste Management Office of Nuclear Regulatory Research U.S. Nuclear Regulatory Commission Washington, D.C. 20555				6. (Leave blank)	
13. TYPE OF REPORT technical report (M.S. thesis)				7. (Leave blank)	
15. SUPPLEMENTARY NOTES				8. (Leave blank)	
16. ABSTRACT (200 words or less) <p>The translational motion as well as the internal motions of the tornado combine to produce the forces experienced by a structure. The combined wind flow and damage patterns are investigated in a series of numerical simulations. The results have been studied and organized on the basis of characteristic properties. Analysis of the damage patterns generated by the simulated tornado wind fields are performed and compared with actual, observed tornado damage patterns. An attempt has been made to categorize tornado damage patterns so that they might be used in field investigations of tornado damage. Various hypothetical sequences of tornado development and behavior are proposed to simulate the resulting tornado damage patterns.</p>				9. (Leave blank)	
17. KEY WORDS AND DOCUMENT ANALYSIS				10. PROJECT/TASK/WORK UNIT NO.	
17b. IDENTIFIERS/OPEN-ENDED TERMS				11. CONTRACT NO. NRC FIN B6177 NRC-04-77-106	
18. AVAILABILITY STATEMENT Unlimited		19. SECURITY CLASS (This report) Unclassified		21. NO. OF PAGES	
		20. SECURITY CLASS (This page) Unclassified		22. PRICE \$	

8203040180

UNITED STATES
NUCLEAR REGULATORY COMMISSION
WASHINGTON, D. C. 20555

OFFICIAL BUSINESS
PENALTY FOR PRIVATE USE, \$300

POSTAGE AND FEES PAID
U.S. NUCLEAR REGULATORY
COMMISSION



120555078877 2 ANRBR6
LS NRC
ADM DIV OF TIDC
POLICY & PUBLICATIONS MGT BR
PDR NUREG COPY
LA 212
WASHINGTON DC 20555

NUREG/CR-2557

SIMULATED TORNADO WIND FIELDS AND DAMAGE PATTERNS

FEBRUARY 1982